THE GEOLOGICAL SOCIETY OF AMERICA®

Rapid migration of a magma source from mid- to deep-crustal levels: Insights from restitic granulite enclaves and anatectic granite

Kai Zhao†, Xisheng Xu§, Saskia Erdmann†, Lei Liu†, and Yan Xia†
State Key Laboratory for Mineral Deposits Research, School of Earth Sciences and Engineering, Nanjing University, Nanjing 210023, China

ABSTRACT

Granulite enclaves as an indicator that can be used to unravel multistage metamorphic histories of orogenic belts have attracted a lot of attention. Few exposed granulite enclaves, however, form restite-melt pairs with their host rocks, which provide unique insight into magma source character and conditions of partial melting. In this study, the orthopyroxene- and plagioclase-rich and the garnet-rich and plagioclase-poor restitic granulite enclaves hosted by three peraluminous granitic plutons from South China were characterized. Mineral assemblages, mineral compositions, pressure-temperature pseudosection modeling, and zircon U-Pb data for the two types of restitic enclaves reveal that (1) an early (255–249 Ma) melting event occurred at conditions of ~950 ± 30 °C and ~500 ± 80 MPa, and (2) a later (245–246 Ma) melting event occurred at conditions of ~905 ± 15 °C and ~675 ± 25 MPa. The crustal magma source is inferred to have rapidly (within 3–10 m.y.) migrated from mid- to deep-crustal levels from ~18 to ~25 km (for an average crustal density of 2.7 g/cm^3), with burial rates of 0.07–0.23 cm yr^{-1}, in response to a switch in the geodynamic regime from subduction to continent-continent collision. Whole-rock elemental and isotopic compositions of enclaves and granitic rocks further indicate that partial melting in the source was nonmodal. The key implications from our findings are that magma sources may migrate over the lifetime of many composite, upper-crustal intrusions, and that compositional variation in intrusive suites may reflect source partial melting at various pressures in addition to other factors.

INTRODUCTION

From field-based studies, experiments, and numerical modeling, it is well established that crustal magma may form at a range of pressures (300–1000 MPa), temperatures (700–1100 °C), system H_2O contents (<0.5 to >10 wt%), and from a range of rock types, e.g., metagraywacke, metapelite, or amphibolite (Vielzeuf and Holloway, 1988; Vielzeuf and Montel, 1994; Patiño-Douce and Beard, 1996; Rapp and Watson, 1995). Melting temperature, melt H_2O content, and thus melt production in a single source may rapidly vary through time; e.g., low-degree partial melting may be followed by high-degree partial melting within ~5 m.y. (sequential melting; Holtz and Barbey, 1991; Neiva et al., 2011; Carvalho et al., 2012). Upper-crustal magma reservoirs may rapidly (within <<1 m.y.) migrate as a function of variation in tectonic stress or magma (and mostly volatile) composition (e.g., Manley and Bacon, 2000; Borgia et al., 2005; Scaillet et al., 2008). It is practically unknown if magma sources in these cases also rapidly migrate, however, due to the scarcity of pressure constraints for magma sources of exposed plutons or volcanic rocks. In theory, a magma source region may actively migrate in response to a geodynamic switch from subduction to collision or syncollision to postcollision. Alternatively, if source melting is partly or largely controlled by the heat derived from injections of mantle-derived magma, then a switch in emplacement depth of the mantle-derived magma will likely also cause a migration of the crustal source.

Compositional variation in igneous suites may reflect that their original magma batches were generated by partial melting at variable pressures, but they may equally reflect the variation of other intensive parameters in the source and/or during crystallization, i.e., equilibrium to nonmodal partial melting, magma mixing, or country-rock assimilation (Clemens and Droop, 1998; Zeng et al., 2005; Stevens et al., 2007; Kemp et al., 2007; Erdmann et al., 2009; Acosta-Vigil et al., 2010). Isotopically homogeneous igneous suites may be derived from a single source, but they may also be derived from two or more sources with equivalent isotopic, yet variable elemental composition, or they may be derived from sources with variable elemental and isotopic composition from which extracted melt batches were well mixed (e.g., Gerdes, 2001). Petrological and geochemical studies and numerical modeling may rule out some parameters and constrain others, but they cannot unequivocally constrain all intensive parameters of a magma system and the magma source in particular. Constraints on intensive source parameters—pressure, temperature, and rock type—require direct evidence in the form of restite, which is rare.

Here, we present a study on two types of restitic granulite enclaves hosted by three peraluminous granitic plutons, the Taima, Dasi, and Jiuzhou plutons in southern China (Fig. 1). The granulite enclaves provide us with an exceptional example, because they comprise mineralogically, geochemically, and isotopically variable enclaves that are hosted by compositionally variable, yet isotopically homogeneous granitic plutons. The enclaves have pressure-temperature (*P-T*)–sensitive assemblages, and they therefore permit us to derive constraints on the conditions of source partial melting, while the elemental and isotopic compositions of both enclaves and their host granitic plutons can be used to constrain equilibrium versus nonmodal partial melting. This study shows that the enclaves and their host plutons record (1) the migration of the crustal magma source from a depth of ~18 to ~25 km within 3–10 m.y. and partial melting at high temperatures of >900 °C; (2) magma generation from sources with contrasting composition and mineralogy yet comparable isotopic composition; and (3) partial melting at variable degrees of isotopic disequilibrium.

GEOLOGICAL BACKGROUND

Qinzhou Bay Granitic Complex in South China

The South China block consists of two subblocks, the Yangtze subblock in the northwest and the Cathaysia subblock in the southeast (Fig. 1). The two subblocks are inferred to have amalgamated in the Neoproterozoic at ca. 825 Ma (Zhao, 2014). The South China block was pervasively folded and faulted and in-

†Zhao—kaivino920@hotmail.com; Erdmann—serdmann@dal.ca; Liu—aliuleiz@gmail.com; Xia—xia_bruce@126.com.
§Corresponding author: xsxu@nju.edu.cn.

GSA Bulletin; November/December 2017; v. 129; no. 11/12; p. 1708–1725; https://doi.org/10.1130/B31462.1; 13 figures; 5 tables; Data Repository item 2017287; published online 18 July 2017.

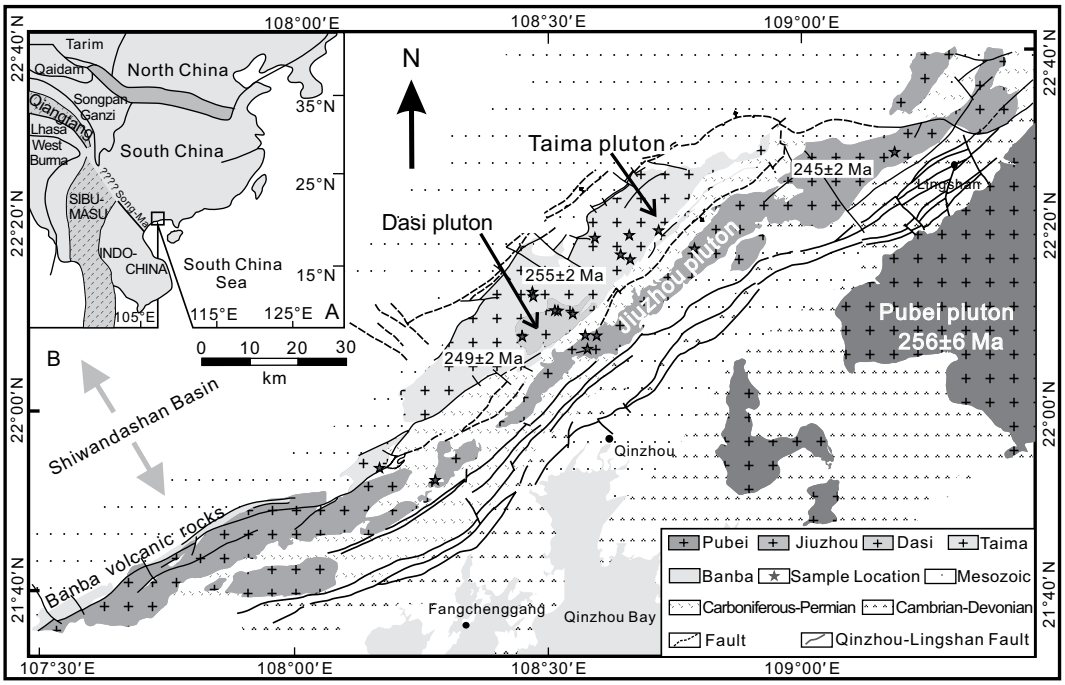

Figure 1. (A) Tectonic schematic map of South China and its surrounding plates (after Carter et al., 2001). (B) Geological map of the Jiuzhou, Taima, and Dasi plutons with sample locations. Ages indicated are U-Pb zircon ages determined in this study for the Taima, Dasi, and Jiuzhou plutons, and U-Pb zircon ages determined for the Pubei pluton by Chen et al. (2011). All four plutons intrude Paleozoic, low-grade metasedimentary rocks, including meta-slates, meta-sandstone and meta-shales, and metamorphic siliceous and carbonate rocks (BGMRGX, 1985; Zhao et al., 2012).

truded by voluminous granites as a result of the Indosinian orogeny during the Late Permian to Triassic (Shu et al., 2008; Chen et al., 2011; Li et al., 2016). The Qinzhou Bay granitic complex in South China, consisting of several granitic plutons and minor volcanic rocks, experienced voluminous magmatism during the Permian to Triassic between 265 and 249 Ma (Jiao et al., 2015; Li et al., 2016). The granitic plutons have strongly peraluminous composition, and they are cordierite-bearing units, indicating predominantly crustal magma sources and low emplacement pressures (≤300 MPa; Zhao et al., 2017). The granitic plutons intrude Paleozoic, low-grade metasedimentary rocks, including meta-slates, meta-sandstone and meta-shale, and metamorphic siliceous and carbonate rocks (Zhao et al., 2012).

Previous Studies on Granulite Enclaves from the Jiuzhou Pluton

The granitic plutons in the Qinzhou Bay granitic complex contain abundant metasedimentary enclaves, including schist, hornfels, and granulite enclaves. Granulite enclaves from the Jiuzhou pluton, but not from the Taima and Dasi plutons, have been previously studied by Zhao et al. (2010, 2102) and Jiao et al. (2013). Zhao et al. (2010, 2102) constrained their metamorphic age to ca. 253 ± 3 Ma and used whole-rock major- and trace-element and Sr-Nd isotopic data to infer a metasedimentary origin and source partial melting conditions of 750–800 MPa and 950–1000 °C. Jiao et al. (2013) conducted phase equilibrium modeling to infer a range of *P-T* crystallization conditions for subassemblages of the studied enclaves. They suggested that partial melting took place at 720–800 MPa and 800–830 °C, that decompression is recorded by orthopyroxene-bearing symplectite at 460–520 MPa and 810–860 °C, and that re-equilibration of the enclaves during magma residence records conditions of 310–380 MPa and 850 °C.

SAMPLES AND ANALYTICAL METHODS

The granulite enclaves and their host granitic plutons were investigated in the field in a total of 18 outcrops. Mineral compositions of orthopyroxene, garnet, and plagioclase were determined for 19 granitic rock samples and for 11 granulite enclave samples using a JEOL JXA-8800 electron microprobe at the State Key Laboratory for Mineral Deposits Research at Nanjing University, Nanjing, China. Details of the analytical procedures are outlined in the supplementary file DR1,[1] and the data are reported in Tables 1–3. X_{Mg} for orthopyroxene and X_{Mg} and X_{Ca} for garnet were calculated as the molar ratio of atoms (X_{Mg} = Mg/[Fe + Mg], X_{Ca} = Ca/[(Fe + Mg + Ca + Mn]), while X_{Al} for orthopyroxene was calculated as the molar atoms (X_{Al} = Al).

Whole-rock composition was determined for 19 granitic rock samples and for three granulite enclave samples. The granulite enclaves have macroscopically sharp contacts against their host granitic rocks (Fig. DR1 in supplementary file [see footnote 1]). Additional granulite enclaves were considered for analysis, but their volume was too small (<~20 cm^3) for a meaningful characterization, or they showed microscale melt veins close to their margin, while their mineral assemblage and mineral composition were comparable to those of the three analyzed samples. We therefore suggest that the analyzed samples are representative of the exposed enclave populations. To rule out the effect of possible contamination by granitic components, e.g., infiltrated into the enclaves as a melt, only central zones were prepared for the whole-rock geochemical analysis. Microscale evidence for reaction between the enclaves and their host magma (e.g., rehydration reactions that produced biotite) was also carefully considered, but not detected, as reported later herein (see

[1]GSA Data Repository item 2017287, analytical methods for mineral geochemistry (Text DR1), bulk rock major-, trace-element and Sr-Nd isotope geochemistry (Text DR2-3), and zircon dating and Hf isotope geochemistry (Text DR3-4); Supplementary figures including field photography for granulite enclaves and their host granite (Fig DR1), microphotograph showing the boundary between the granulite enclaves and their granite host (Fig DR2), geochronological data including the U-Pb concordia diagram (Fig DR3) and zircon CL images (Fig DR4), and T-XH_2O and P-T pseudosections with supplementary information for Fig. 8 in the text (Fig DR5), Supplementary tables including coordinates of the collected samples (Table DR1), and U-Th-Pb-Hf isotope data for zircon (Table DR2-3), is available at http://www.geosociety.org/datarepository/2017 or by request to editing@geosociety.org.

TABLE 1. REPRESENTATIVE ELECTRON MICROPROBE DATA FOR ORTHOPYROXENE IN GRANULITE ENCLAVES AND HOST GRANITE

	In granulite enclaves						In granite				
Sample	DS04-2		JZ02-3	JZ01-2		JZ01-2	JZ01-1		JZ09		
SiO_2	52.61	52.22	46.83	49.50	48.15	50.41	50.79	53.19	46.21	49.63	50.82
TiO_2	0.18	0.19	0.13	0.18	0.14	0.20	0.18	0.02	0.17	0.06	0.19
Al_2O_3	1.21	0.67	3.14	4.48	3.47	1.13	0.91	0.51	1.00	0.69	0.81
FeO	21.50	20.57	36.92	32.16	34.60	29.96	31.32	32.26	37.18	36.66	34.25
MnO	0.33	0.37	0.48	0.44	0.59	0.43	0.46	0.91	0.68	0.75	0.96
MgO	23.60	24.25	11.49	12.46	13.76	18.13	15.25	13.17	13.02	12.63	12.54
CaO	1.02	0.90	0.17	0.14	0.11	0.22	0.19	0.07	0.21	0.11	0.15
Na_2O	0.02	0.03	0.00	0.07	0.03	0.03	0.00	0.13	0.00	0.04	0.03
K_2O	0.00	0.02	0.01	0.03	0.00	0.00	0.00	0.04	0.00	0.00	0.00
Total	100.48	99.21	99.16	99.46	100.85	100.51	99.09	100.28	98.46	100.56	99.75
On the basis of four cations per six oxygens											
Si	1.935	1.937	1.888	1.960	1.880	1.927	2.001	2.096	1.871	1.969	2.027
Ti	0.005	0.005	0.004	0.005	0.004	0.006	0.005	0.001	0.005	0.002	0.006
^{IV}Al	0.053	0.029	0.112	0.040	0.120	0.051	0.000	0.000	0.048	0.031	0.000
^{VI}Al	0.000	0.000	0.037	0.169	0.039	0.000	0.042	0.023	0.000	0.001	0.038
Fe(iii)*	0.068	0.088	0.067	0.000	0.075	0.085	0.000	0.000	0.201	0.029	0.000
Fe(ii)	0.593	0.550	1.178	1.065	1.054	0.873	1.032	1.063	1.058	1.188	1.143
Mn	0.010	0.012	0.016	0.015	0.019	0.014	0.015	0.030	0.023	0.025	0.032
Mg	1.294	1.341	0.690	0.735	0.801	1.033	0.896	0.774	0.786	0.747	0.746
Ca	0.040	0.036	0.007	0.006	0.005	0.009	0.008	0.003	0.009	0.005	0.006
Na	0.001	0.002	0.000	0.006	0.002	0.002	0.000	0.010	0.000	0.003	0.003
X_{Mg}	0.66	0.68	0.36	0.41	0.42	0.52	0.47	0.42	0.39	0.38	0.40
X_{Al}	0.02	0.01	0.06	0.09	0.07	0.02	0.02	0.01	0.02	0.01	0.02

Note: Fe^{3+} is calculated from charge balance. Major elements are given in wt%.

TABLE 2. REPRESENTATIVE ELECTRON MICROPROBE DATA FOR GARNET IN GRANULITE ENCLAVES AND HOST GRANITE

Sample	In granulite enclaves					In granite					
	JZ01-2		JZ02-1	JZ02-3		DS03 (in crystal clusters)					
Remarks	Core	Rim	Core	Core	Rim	Rim		Core		Rim	
SiO_2	37.08	37.44	37.28	36.913	36.85	38.42	37.78	38.66	38.22	38.76	39.19
TiO_2	0.00	0.02	0.02	0.00	0.13	0.00	0.05	0.01	0.07	0.03	0.01
Al_2O_3	23.61	23.64	22.14	21.79	23.14	20.81	20.72	21.10	20.95	20.78	21.01
FeO	31.45	32.21	32.41	34.41	35.65	31.71	31.53	31.42	31.47	31.37	31.79
MnO	1.65	1.75	1.03	0.23	1.48	1.35	1.31	1.37	1.21	1.38	1.33
MgO	4.69	4.11	6.88	4.71	3.61	6.12	6.43	6.60	6.33	6.43	5.85
CaO	1.25	1.26	1.02	1.58	1.40	1.57	1.50	1.50	1.46	1.50	1.53
Na_2O	0.00	0.02	0.05	0.02	0.04	0.03	0.03	0.02	0.02	0.00	0.03
K_2O	0.02	0.02	0.02	0.02	0.00	0.00	0.01	0.01	0.00	0.00	0.00
Cr_2O_3	0.00	0.00	0.00	0.00	0.00	0.14	0.15	0.13	0.13	0.13	0.09
Total	99.74	100.46	100.85	99.68	100.13	100.15	99.49	100.82	99.85	100.38	100.84
On the basis of eight cations per twelve oxygens											
Si	2.939	2.959	2.904	2.945	3.751	3.031	2.996	3.020	3.018	3.044	3.073
Ti	0.000	0.001	0.001	0.000	0.010	0.000	0.003	0.001	0.004	0.002	0.001
Al	2.205	2.203	2.032	2.049	0.376	1.935	1.936	1.942	1.950	1.923	1.942
Cr	0.000	0.000	0.000	0.000	0.000	0.000	0.000	0.000	0.000	0.000	0.000
Fe(iii)	0.000	0.000	0.158	0.062	0.102	0.004	0.067	0.017	0.005	0.000	0.000
Fe(ii)	2.085	2.129	1.954	2.234	2.933	2.088	2.024	2.035	2.074	2.060	2.084
Mn	0.111	0.117	0.068	0.016	0.127	0.090	0.088	0.091	0.081	0.092	0.088
Mg	0.554	0.484	0.799	0.560	0.548	0.720	0.759	0.769	0.745	0.753	0.684
Ca	0.106	0.107	0.085	0.135	0.153	0.133	0.127	0.125	0.123	0.126	0.128
Almandine	73.02	75.04	67.24	76.37	77.99	68.89	67.50	67.38	68.61	67.97	69.83
Pyrope	19.40	17.06	27.50	18.62	14.56	23.76	25.33	25.46	24.64	24.83	22.92
Grossular	3.71	3.77	2.71	4.49	3.13	4.37	4.10	4.12	4.06	4.17	4.30
Spessartine	3.87	4.13	2.33	0.52	3.39	2.98	2.92	3.01	2.68	3.03	2.95

Note: Fe^{3+} is calculated from charge balance. Major elements are given in wt%.

"Granulite Enclaves" subsection of the "Petrography and Mineral Composition" section). Whole-rock major- and trace-element analyses were performed using an ARL9800XP+ X-ray fluorescence spectrometer (XRF) and a Finnigan Element II inductively coupled plasma mass spectrometer (ICP-MS), respectively, at the State Key Laboratory for Mineral Deposits Research, Nanjing University, Nanjing, China. Details of the analytical procedures are summarized in the supplementary file DR2 (see footnote 1), and the data are shown in Table 4. The Sr and Nd isotopic compositions of six granitic rock samples and three granulite enclave samples were measured using a Finnigan Triton TI thermal ionization mass spectrometer (TIMS) and a Neptune (Plus) multicollector (MC) ICP-MS at the State Key Laboratory of Mineral Deposits Research, Nanjing University. The details of the analytical procedures are reported in the supplementary file DR3 (see footnote 1), and the data are shown in Table 5.

Zircon U-Pb isotopes for four granitic rocks were analyzed at the State Key Laboratory for Mineral Deposits Research, Nanjing University, using an Agilent 7500a ICP-MS attached to a New Wave 213 nm laser-ablation system with an in-house sample cell. The in situ Lu-Hf isotopic analyses of zircon were conducted using a Neptune Plus plasma MC-ICP-MS equipped with a UP 193 nm laser sampler at the State Key Laboratory for Mineral Deposits Research, Nanjing University. Details of the

TABLE 3. REPRESENTATIVE ELECTRON MICROPROBE DATA FOR PLAGIOCLASE IN GRANULITE ENCLAVES AND HOST GRANITE

	In granulite		In granite		
Sample	JZ02-3	DS04-2	DS03		TM07
SiO_2	56.18	45.97	55.73	60.76	57.88
TiO_2	0.04	0.02	0.00	0.00	0.05
Al_2O_3	27.76	33.06	28.69	25.70	27.41
FeO	0.12	0.23	0.09	0.11	0.06
MnO	0.05	0.02	0.02	0.00	0.00
MgO	0.00	0.02	0.03	0.00	0.01
CaO	10.73	18.45	9.70	6.04	7.46
Na_2O	5.76	1.16	5.41	6.89	6.92
K_2O	0.10	0.07	0.72	0.54	0.42
Total	100.73	98.99	100.38	100.05	100.20
On the basis of five cations per eight oxygens					
Si	2.511	2.143	2.500	2.720	2.579
Ti	0.001	0.001	0.000	0.000	0.002
Al	1.462	1.816	1.517	1.356	1.439
Fe(ii)	0.004	0.009	0.003	0.004	0.002
Mn	0.002	0.001	0.001	0.000	0.000
Mg	0.000	0.002	0.002	0.000	0.000
Ca	0.514	0.921	0.466	0.290	0.356
Na	0.499	0.104	0.470	0.598	0.598
K	0.006	0.004	0.041	0.031	0.024
An	50.42	89.47	47.70	31.54	36.43
Ab	49.00	10.14	48.12	65.10	61.15
Or	0.58	0.39	4.18	3.36	2.42

Note: Major elements are given in wt%.

analytical procedures are given in the supplementary file DR4, while the data are shown in file DR5 (see footnote 1).

PETROGRAPHY AND MINERAL COMPOSITION

Granulite Enclaves

In the studied plutons, schist, hornfels, and granulite enclaves are present. These enclaves are variably abundant, with 10–20 vol% per square meter to near absence. Granulite enclaves are relatively rare, making up <2 vol% overall. The granulite enclaves are dark gray in hand specimen. They are subrounded, they typically have maximum dimensions between several centimeters and decimeters, and they are unzoned in color and grain size (supplementary Fig. DR1 [see footnote 1]). Microscale observations show that the enclaves have sharp contacts against the granitic host rocks. There also is no evidence for the injection of granitic microveins or rehydration reactions (e.g., that produced biotite; Fig. DR2 [see footnote 1]). However, the effect of mineral-scale diffusive reequilibration will be further considered in the "Phase Equilibrium Modeling" section).

Based on their mineralogy, the granulite enclaves can be divided into two groups. One group of enclaves, hereafter termed "Opx- and Pl-rich enclaves," is predominantly composed of orthopyroxene (Opx), plagioclase (Pl), ilmenite, quartz, biotite, and clinopyroxene (a representative sample is DS04-2 collected from the Dasi pluton; Fig. 1). The crystals are subhedral to highly anhedral, where most grain boundaries are cuspate-lobate or irregularly segmented (Fig. 2A). Plagioclase and orthopyroxene account for ~50 vol% and ~25 vol% of the phases, respectively. Quartz and ilmenite, respectively, account for ~20 vol% and <3 vol% of the assemblage, while clinopyroxene, biotite, and alkali feldspar form minor constituents (<1–3 vol%). Orthopyroxene forms a crystalloblastic texture with plagioclase and ilmenite. Orthopyroxene is predominantly subhedral and unzoned, and its composition is characterized by high X_{Mg} values (0.66–0.68) and a relatively low Al_2O_3 content (0.67–1.21 wt%; Fig. 3A; Table 1). Plagioclase is prismatic, typically with anhedral grain boundaries against quartz and orthopyroxene. Plagioclase is unzoned, and it has a high X_{An} content (~0.90; Table 3). Ilmenite forms subhedral crystals, while clinopyroxene forms subrounded crystals that commonly enclose biotite. Alkali feldspar with anhedral to subhedral shape forms a minor constituent. Quartz is always anhedral and interstitial.

The second group of enclaves, hereafter termed "Grt-rich and Pl-poor granulite enclaves," consists mainly of garnet (Grt; 20–25 vol%), cordierite (40–50 vol%), spinel (5–8 vol%), biotite (8–10 vol%), orthopyroxene (<5 vol%), alkali feldspar (8–10 vol%), plagioclase (<3 vol%), and ilmenite (<2 vol%; representative samples are JZ01-2 and JZ02-3 collected from the Jiuzhou pluton; Fig. 1). Garnet with grain sizes of 1–2 mm forms subhedral to anhedral porphyroblasts with irregular grain boundary outlines and contains abundant biotite and sillimanite inclusions (Fig. 2B). The crystals have almandine- and pyrope-rich (Alm: 67–78 wt%, Prp: 14–28 wt%), and grossular- and spessartine-poor (Grs: 3–5 wt%, Sps: <4 wt%) compositions. They show weak normal zoning with a narrow rim <100 μm, where core and rim X_{Mg} values vary from 0.19 to 0.28 and from 0.14 to 0.17, respectively (Table 2). They have mantles of cordierite + orthopyroxene symplectite that are up to ~600 μm wide (Fig. 2B). Orthopyroxene in the symplectite from different samples is unzoned and has low X_{Mg} (X_{Mg} = 0.36–0.52) and high Al_2O_3 content (1.1–4.5 wt%; Fig. 3A). The matrix of the enclaves consists mainly of cordierite, spinel, and sillimanite, with subordinate plagioclase, biotite, and ilmenite (Fig. 2C). Cordierite forms single, subhedral crystals against grain boundaries of garnet or intergrowths with anhedral to subhedral spinel. Biotite often forms subhedral-euhedral inclusions in garnet, cordierite, or alkali feldspar. Plagioclase forms rare subhedral crystals with an X_{An} content of ~0.5.

Granitic Rocks

The rocks of the Taima pluton are porphyritic with a phenocryst content of up to 40–50 vol% (Fig. 2D). The phenocrysts include plagioclase (30–37 vol%), quartz (30–35 vol%), alkali feldspar (25–30 vol%), orthopyroxene (<1 vol%), biotite (<3 vol%), and cordierite (<3 vol%) with maximum dimensions of ~2 cm. They are set in a matrix of plagioclase, alkali feldspar, quartz, and biotite, with accessory zircon, monazite, apatite, and ilmenite. The maximum crystal size of the matrix minerals is <50 μm. Alkali feldspar and plagioclase are commonly broken, exhibiting an autoclastic texture. Quartz typically shows subrounded and embayed shapes. All of these textural features suggest a subvolcanic origin. Cordierite forms euhedral phenocrysts, but they are partially altered to chlorite, serpentine, or sericite (Fig. 2D). Biotite is present either as a phenocryst phase or in the matrix with maximum dimensions of <0.1–1 mm. Crystal clusters of orthopyroxene + plagioclase + ilmenite with irregular shapes and sizes up to ~3 mm are also present in the Taima pluton (Fig. 4A). They have a crystalloblastic texture and minerals with anhedral shape. They are thus mineralogically and texturally different from the main granite phenocryst assemblage, but they are comparable to the assemblage and the texture of the Opx- and Pl-rich granulite enclaves (Fig. 4A). The clusters generally make up less than ~3 vol%, and they are absent from some samples. The orthopyroxene in the cluster has moderately low X_{Mg} (X_{Mg} = 0.43–0.44) and high Al_2O_3 content (3.37–4.41 wt%; Table 1).

TABLE 4. MAJOR- (WT%) AND TRACE-ELEMENT (PPM) COMPOSITIONS FOR GRANITE AND GRANULITE ENCLAVES

	Taima pluton									Dasi pluton			Jiuzhou pluton							Granulite enclaves		
Sample	TM01	TM03	TM04	TM05	TM06	TM07	TM08	TM09	TM10	DS02	DS03	DS04-1	JZ01-1	JZ03-4	JZ04	JZ05-1	JZ06-1	JZ09	JZ10	DS04-2	J201-2	JZ02-3
SiO_2	74.32	70.67	72.13	73.08	71.67	71.11	72.09	73.18	72.56	68.76	68.71	69.64	62.95	65.66	69.13	70.32	69.91	67.41	68.63	55.54	44.96	48.76
TiO_2	0.29	0.34	0.38	0.34	0.39	0.46	0.37	0.33	0.35	0.65	0.70	0.61	1.11	0.88	0.75	0.59	0.66	0.89	0.74	0.68	1.28	1.02
Al_2O_3	13.81	14.16	14.56	14.42	14.16	14.90	14.56	14.35	14.27	14.34	14.40	14.36	15.63	15.32	13.86	14.09	13.81	14.58	14.05	18.44	30.50	26.74
Fe_2O_3	1.69	2.17	2.47	2.10	2.36	2.93	2.28	1.94	2.13	4.37	4.68	4.01	7.06	5.72	5.09	4.00	4.92	5.83	5.15	8.38	10.70	10.13
MnO	0.03	0.04	0.04	0.03	0.04	0.04	0.03	0.04	0.03	0.06	0.06	0.05	0.09	0.07	0.06	0.05	0.06	0.08	0.07	0.10	0.06	0.12
MgO	0.38	0.57	0.61	0.58	0.62	0.85	0.53	0.50	0.45	1.30	1.39	1.17	2.16	1.80	1.70	1.51	2.04	1.78	1.64	5.70	5.80	4.62
CaO	1.78	1.90	2.52	1.86	1.96	2.24	2.26	1.69	2.09	2.48	2.69	2.62	3.64	3.18	2.06	1.69	1.52	3.00	2.46	6.87	0.83	1.64
Na_2O	2.37	2.14	2.48	2.77	2.36	2.44	2.26	2.54	2.37	2.19	2.31	2.31	2.29	2.15	1.90	1.95	1.97	2.16	2.23	1.89	0.66	1.50
K_2O	5.06	5.26	4.51	4.88	5.13	4.87	4.94	5.25	4.87	4.30	4.14	4.21	3.43	3.36	3.89	4.01	3.58	3.60	3.56	0.63	2.38	3.30
P_2O_5	0.13	0.13	0.13	0.13	0.14	0.15	0.14	0.13	0.14	0.15	0.16	0.15	0.16	0.18	0.15	0.15	0.15	0.16	0.15	0.07	0.13	0.19
LOI	0.78	1.49	0.70	0.77	0.94	0.69	0.62	0.82	0.74	1.00	0.55	1.05	1.17	1.27	1.17	1.65	1.45	0.55	1.05	2.43	2.92	1.07
Total	100.64	98.87	100.52	100.95	99.76	100.67	100.08	100.75	100.00	99.60	99.79	100.19	99.70	99.59	99.77	99.99	100.07	100.04	99.73	100.73	100.23	98.20
A/CNK	1.09	1.12	1.07	1.09	1.09	1.11	1.10	1.11	1.10	1.12	1.09	1.09	1.11	1.18	1.25	1.32	1.40	1.13	1.17	1.13	5.89	2.96
Li	38.9	41.0	43.1	59.2	31.6	43.5	44.0	45.5	33.3	40.0	37.9	39.6	32.6	37.6	46.1	48.3	40.6	38.8	40.6	47.5	92.0	97.9
Be	2.64	2.61	2.50	2.54	2.44	2.88	2.59	2.65	2.59	2.34	2.38	2.43	1.70	3.36	2.14	2.25	2.62	2.30	2.00	2.21	2.45	2.05
Sc	4.05	4.73	5.71	5.07	5.02	6.25	4.30	4.51	4.81	10.48	10.91	9.36	16.81	13.19	11.40	8.90	10.94	14.08	11.41	26.18	22.11	23.38
Ti	1725	2022	2258	1965	2270	2603	1932	1957	2063	3695	4072	3531	5987	5028	4227	3339	3736	4957	4219	3991	7351	6404
V	16.9	23.4	26.0	23.3	25.4	34.0	21.8	20.6	23.3	51.4	52.9	49.5	99.0	90.9	67.7	57.5	79.4	78.3	68.4	150.1	239.9	117.6
Cr	11.7	13.8	17.6	27.2	56.5	28.2	12.3	17.8	13.9	34.8	43.4	33.1	61.0	72.2	54.3	50.7	78.2	54.0	56.5	130.8	172.2	151.8
Mn	442	550	656	485	301	719	587	613	543	1025	1073	904	1561	1209	1071	785	1080	1425	1059	1183	649	2161
Co	3.12	4.19	5.15	4.52	6.35	6.18	3.54	3.72	4.21	10.3	11.9	9.74	16.0	13.9	13.4	11.1	15.0	15.1	12.4	26.3	46.5	26.6
Ni	5.75	6.44	7.46	13.2	11.1	10.8	5.72	12.6	6.46	18.9	26.2	19.7	31.4	40.1	31.0	29.8	43.9	32.7	33.3	30.5	107.5	61.5
Cu	7.82	9.40	9.78	8.97	6.10	10.5	8.79	10.5	9.82	17.5	21.0	20.7	27.9	30.6	25.2	24.3	27.4	24.6	23.6	18.5	199.8	7.01
Zn	46.9	43.2	42.7	45.7	54.6	57.9	42.3	52.3	49.3	66.1	80.2	81.8	100	84.6	86.1	68.0	79.8	88.6	87.7	114.7	305.7	168
Ga	17.5	17.2	17.8	17.9	17.0	18.5	17.3	17.9	17.6	18.2	19.0	18.5	21.0	20.4	18.1	17.6	18.1	19.3	18.3	23.3	41.5	40.6
Rb	266	246	198	229	236	228	242	251	238	190	189	185	139	142	186	183	166	169	160	37.8	46.2	86.7
Sr	75.1	76.7	102.1	92.7	90.1	88.2	90.4	92.4	81.3	109.4	106	110	170	135	102	101	88.3	120	125	158	80.3	141
Y	46.1	34.7	31.2	32.0	35.0	34.6	36.6	37.1	35.4	34.0	33.9	33.1	34.3	31.4	28.7	25.3	24.9	34.8	34.5	19.7	18.6	38.6
Zr	175	193	214	158	187	242	185	169	221	311	294	294	507	408	282	255	229	375	288	87.7	234	196
Nb	12.0	12.0	11.9	11.4	16.3	13.5	11.7	12.3	12.4	15.7	16.5	15.2	22.3	19.6	17.8	15.6	16.7	19.5	16.3	10.1	26.4	34.3
Mo	0.44	0.38	0.56	0.34	0.63	0.52	0.21	0.22	0.53	0.79	0.93	0.71	0.80	0.98	0.74	0.57	1.04	1.02	0.72	0.32	1.90	0.19
Sn	7.40	5.88	4.89	5.06	4.29	5.48	5.80	6.03	6.25	4.18	4.17	4.65	3.65	2.95	4.90	4.36	4.08	3.83	3.69	1.01	1.55	0.66
Cs	13.1	11.5	8.72	9.21	10.8	10.6	9.67	9.84	9.40	8.34	8.50	7.79	7.83	8.79	12.3	9.86	11.0	10.2	9.19	8.63	8.18	6.97
Ba	670	888	902	773	771	815	812	790	753	860	786	811	940	956	593	668	669	715	653	208	1941	1906
La	37.1	40.5	42.6	41.9	44.2	43.7	39.7	44.7	40.8	47.8	50.5	49.0	68.2	60.3	43.3	40.0	38.9	50.6	49.3	50.9	78.5	59.8
Ce	71.0	78.7	81.7	80.2	85.4	85.4	76.0	85.8	78.8	91.4	97.2	93.7	129	114	84.9	77.4	75.5	97.9	94.3	95.6	154	117
Pr	8.60	9.20	9.53	9.22	10.1	10.0	9.04	10.1	9.29	10.7	11.4	11.0	14.9	13.3	10.0	9.14	8.88	11.4	11.0	11.2	14.5	13.5
Nd	32.9	35.1	36.2	34.5	37.5	37.7	34.3	38.0	35.2	40.9	43.5	42.6	57.4	50.6	38.2	34.8	34.0	44.3	42.0	44.2	72.7	49.6
Sm	6.89	6.96	6.90	6.57	7.29	7.38	6.94	7.41	7.07	7.72	8.05	7.91	10.0	8.98	7.33	6.66	6.47	8.12	7.81	7.48	13.5	8.68
Eu	1.09	1.23	1.38	1.23	1.23	1.26	1.25	1.29	1.17	1.38	1.37	1.37	1.87	1.76	1.18	1.26	1.20	1.41	1.28	1.15	1.72	2.51
Gd	7.28	6.91	6.75	6.50	7.17	7.25	6.94	7.41	6.95	7.48	7.84	7.66	9.46	8.54	6.99	6.23	6.14	7.94	7.50	6.17	10.8	8.70
Tb	1.29	1.13	1.06	1.05	1.15	1.16	1.16	1.22	1.15	1.16	1.20	1.16	1.32	1.21	1.07	0.92	0.93	1.20	1.15	1.01	1.70	1.33
Dy	8.04	6.63	6.15	6.19	6.64	6.72	6.92	7.15	6.80	6.64	6.63	6.54	6.97	6.48	5.91	4.84	5.07	6.83	6.56	4.91	6.72	7.57
Ho	1.60	1.30	1.16	1.20	1.29	1.30	1.35	1.38	1.31	1.30	1.28	1.26	1.32	1.22	1.10	0.88	0.93	1.33	1.29	0.93	0.95	1.48
Er	4.64	3.75	3.38	3.55	3.78	3.76	3.95	3.99	3.82	3.88	3.73	3.66	3.92	3.51	3.11	2.50	2.70	3.93	3.85	2.37	1.93	4.39
Tm	0.65	0.53	0.48	0.51	0.52	0.53	0.56	0.56	0.54	0.55	0.53	0.52	0.56	0.49	0.43	0.35	0.38	0.57	0.56	0.45	0.26	0.61
Yb	3.93	3.30	3.00	3.22	3.30	3.33	3.44	3.44	3.37	3.60	3.36	3.29	3.76	3.23	2.69	2.17	2.48	3.74	3.63	2.76	1.57	3.86
Lu	0.57	0.49	0.45	0.47	0.49	0.50	0.51	0.50	0.50	0.55	0.51	0.50	0.60	0.51	0.41	0.33	0.38	0.57	0.55	0.38	0.22	0.58
Hf	5.62	6.02	6.42	4.97	5.84	7.34	5.79	5.31	6.81	9.07	8.51	8.54	14.4	11.3	8.39	7.65	6.85	10.8	8.15	2.70	7.37	6.03
Ta	1.03	0.97	0.90	0.90	0.91	1.04	0.96	0.98	1.01	1.09	1.12	1.08	1.38	1.22	1.22	1.17	1.25	1.31	1.10	0.91	2.77	1.85
W	1.80	2.10	1.92	1.16	1.11	2.11	1.86	1.71	2.17	1.54	1.98	1.62	1.45	1.43	1.90	1.90	1.58	1.82	1.66	1.61	1.60	1.63
Pb	29.5	27.6	28.6	28.3	28.5	29.1	28.9	29.7	30.0	28.0	27.8	35.9	23.8	31.4	28.4	28.1	24.2	24.6	24.1	18.4	30.2	27.5
Bi	0.46	0.42	0.32	0.23	0.14	0.25	0.29	0.32	0.42	0.19	0.13	0.25	0.13	0.14	0.25	0.41	0.13	0.26	0.26	0.07	0.26	0.04
Th	23.4	23.2	22.4	21.1	34.0	24.3	22.9	24.0	23.8	23.8	24.9	24.8	29.3	25.6	21.9	19.8	17.6	23.6	23.0	22.2	41.3	40.5
U	7.14	5.57	4.77	5.19	5.35	5.48	5.39	5.49	6.31	4.31	4.21	4.88	3.32	2.77	3.93	5.05	4.94	4.03	4.55	2.17	9.68	3.70
Sm/Nd	0.21	0.20	0.19	0.19	0.19	0.20	0.20	0.20	0.20	0.19	0.18	0.19	0.18	0.18	0.19	0.19	0.19	0.18	0.19	0.17	0.19	0.17
ΣLREE	150	164	170	166	177	177	159	179	164	191	203	196	269	238	176	16	157	204	197	202	320	240
REE	186	196	201	196	210.	210	192	213	197	225	237	230	309	274	207	188	184	240	231	230	359	280
LREE*	1101	1180	1248	1155	1228	1147	1146	1091	1146	1249	1365	1309	404	291	223	180	160	319	274	–	–	–

Note: Major elements are given in wt%, and trace elements are given in ppm. LOI—loss on ignition; LREE—light rare earth elements; REE—rare earth elements. A/CNK = $Al_2O_3/(CaO + Na_2O + K_2O)$. The major element data for TM07, DS02 and JZ01-1 are from Zhao et al. (2017).

TABLE 5. Sr-Nd ISOTOPIC DATA FOR REPRESENTATIVE GRANITE AND GRANULITE ENCLAVE SAMPLES

Sample	Age (Ma)	Rb (ppm)	Sr (ppm)	$^{87}Rb/^{86}Sr$	$^{87}Sr/^{86}Sr$	$(^{87}Sr/^{86}Sr)_i$	Sm (ppm)	Nd (ppm)	$^{147}Sm/^{144}Nd$	$^{143}Nd/^{144}Nd$	$\varepsilon_{Nd}(t)$	T_{2DM} (Ga)
Jiuzhou pluton												
JZ03-4	250	142	135	396	0.732523	0.72153	8.98	50.6	0.1073	0.511898	–11.6	1.96
JZ09	250	169	119	351	0.735089	0.72039	8.12	44.3	0.1109	0.511911	–11.4	1.95
Dasi pluton												
DS03	250	189	105	309	0.740194	0.72143	8.05	43.5	0.1117	0.511912	–11.5	1.95
DS04-1	250	185	109	321	0.739214	0.72157	7.91	42.1	0.1137	0.511928	–11.2	1.93
Taima pluton												
TM04	250	198	102	299	0.740803	0.72052	6.90	36.2	0.1150	0.511928	–11.3	1.94
TM08	250	242	90.4	264	0.746782	0.71874	6.94	34.3	0.1225	0.511944	–11.2	1.93
Granulite enclaves												
DS04-2	250	37.8	158	462	0.728854	0.72636	7.48	44.2	0.1023	0.511830	–12.7	2.06
JZ01-2	250	46.2	80.3	235	0.746197	0.74020	13.5	72.7	0.1125	0.511723	–15.1	2.25
JZ02-3	250	86.7	141	414	0.741502	0.73511	8.68	49.6	0.1057	0.511811	–13.2	2.10

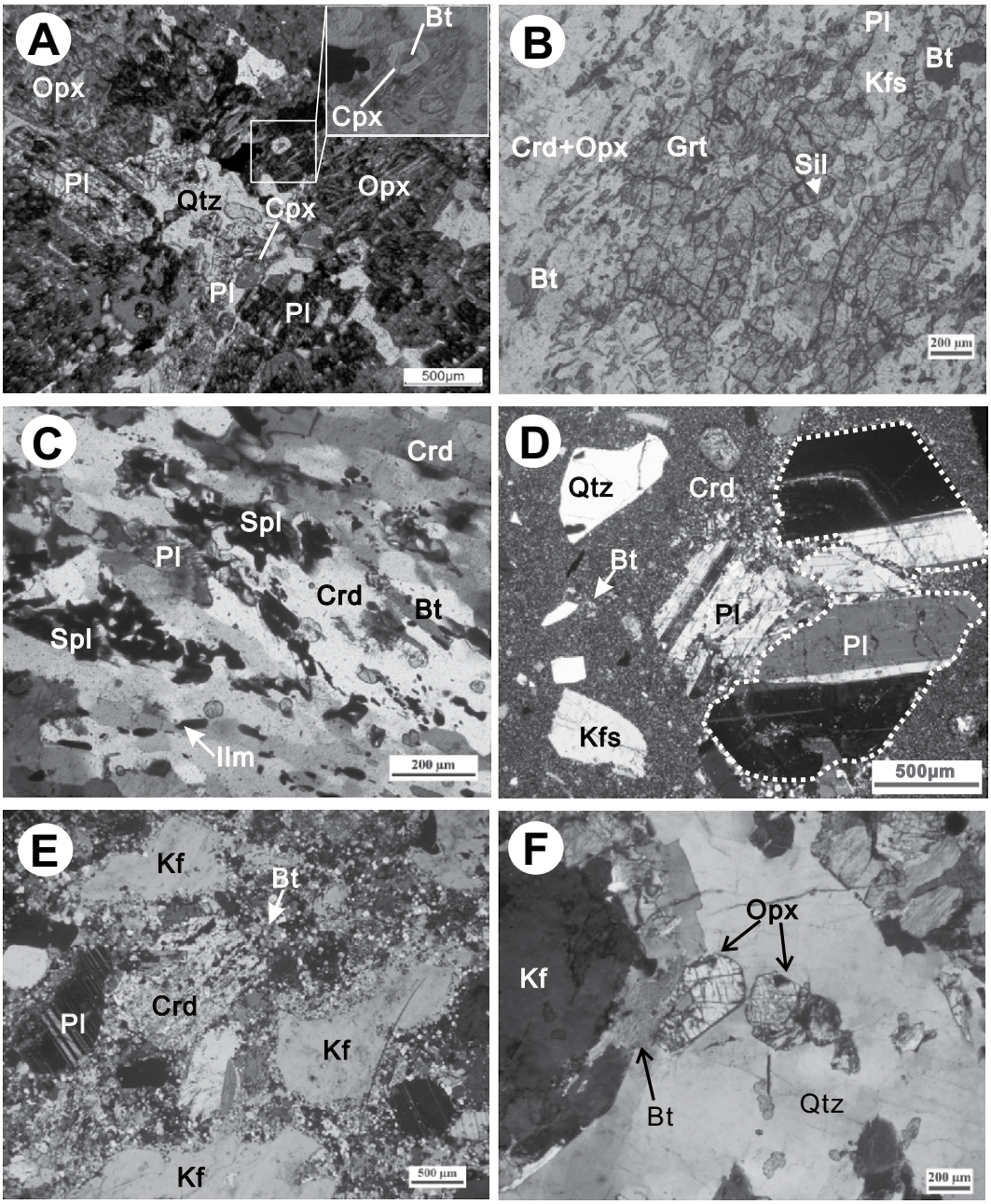

Figure 2. (A–C) Microphotographs of the studied granulite enclaves and the (D) Taima, (E) Dasi, and (F) Jiuzhou granite. Mineral abbreviations are those of Whitney and Evans (2010). (A) Opx- and Pl-rich enclave (DS04-2). Orthopyroxene (Opx), plagioclase (Pl), ilmenite (Ilm), quartz (Qtz), and clinopyroxene (Cpx) form a crystalloblastic texture; quartz occurs as anhedral interstitial crystals. Biotite (Bt) is rare and typically included in clinopyroxene (shown in inset). Clinopyroxene is a minor component (on average ~1 vol%), but it is relatively common in the imaged area. (B) Grt-rich and Pl-poor granulite enclave (JZ02-3). Garnet porphyroblast with biotite and sillimanite (Sil) inclusions and intergrown with K-feldspar (Kf). The garnet crystal is mantled by cordierite (Crd) and orthopyroxene symplectite. (C) Cordierite and spinel (Spl) matrix of the Grt-rich and Pl-poor enclave (JZ02-3). (D) Taima subvolcanic rock with plagioclase, quartz, K-feldspar, and cordierite phenocrysts (~40–50 vol%) in a fine-grained matrix. (E) Dasi subvolcanic rock with an equivalent phenocrysts assemblage to that of the Taima granite, but with a higher phenocryst proportion (~50–60 vol%). (F) Coarse-grained Jiuzhou granite, in which euhedral orthopyroxene forms part of the characteristic assemblage.

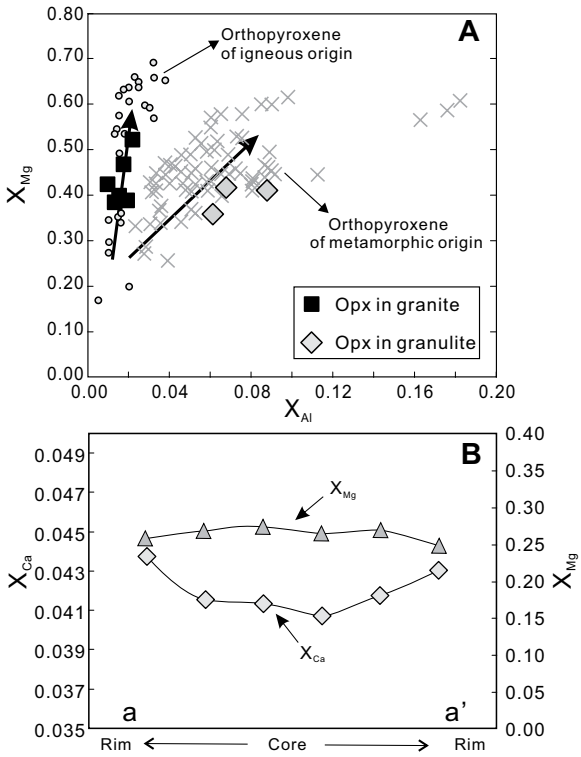

Figure 3. (A) Orthopyroxene X_{Mg} vs. X_{Al} composition. The plot shows our data in comparison to orthopyroxene composition from Rajesh et al. (2011, and references therein). Euhedral orthopyroxene from the Jiuzhou granite is comparable to typical magmatic composition, while orthopyroxene from the garnet-rich and plagioclase-poor enclaves has typical metamorphic composition. (B) Compositional profile for garnet from one of the Grt + Opx + Pl crystal clusters (~1 mm in length; the location of the analytical profile is shown in Fig. 4C).

The Dasi pluton, which is surrounded by rocks of the Taima pluton, has a higher phenocryst content (up to 50–60 vol%) than the Taima granitic rocks. The phenocrysts consist of plagioclase (31–35 vol%), quartz (~30 vol%), alkali feldspar (26–30 vol%), orthopyroxene (~5 vol%), biotite (~3 vol%), and cordierite (~2 vol%), with sizes of 0.25–2 mm (Fig. 2E). The matrix minerals, including quartz, plagioclase, K-feldspar, biotite, and accessories, are equivalent to those of the Taima pluton, but they have larger sizes, up to ~100 μm (Fig. 2E). Crystal clusters of orthopyroxene + plagioclase + ilmenite also occur in the Dasi pluton (Fig. 4B), where they are more abundant (5–10 vol%) than in the Taima pluton. The size, shape, mineral textures, and mineral compositions of the crystal clusters are comparable to those in the Taima pluton. In addition to the orthopyroxene + plagioclase + ilmenite clusters, rare (<1 vol %) crystal clusters composed of garnet + orthopyroxene + plagioclase + ilmenite + quartz are also present in the Dasi pluton (Fig. 4C). These clusters have maximum dimensions of up to ~7 mm, a crystalloblastic texture, and minerals characterized by anhedral shape. They are comparable in mineral assemblage to granulite enclaves from the Jiuzhou pluton described by

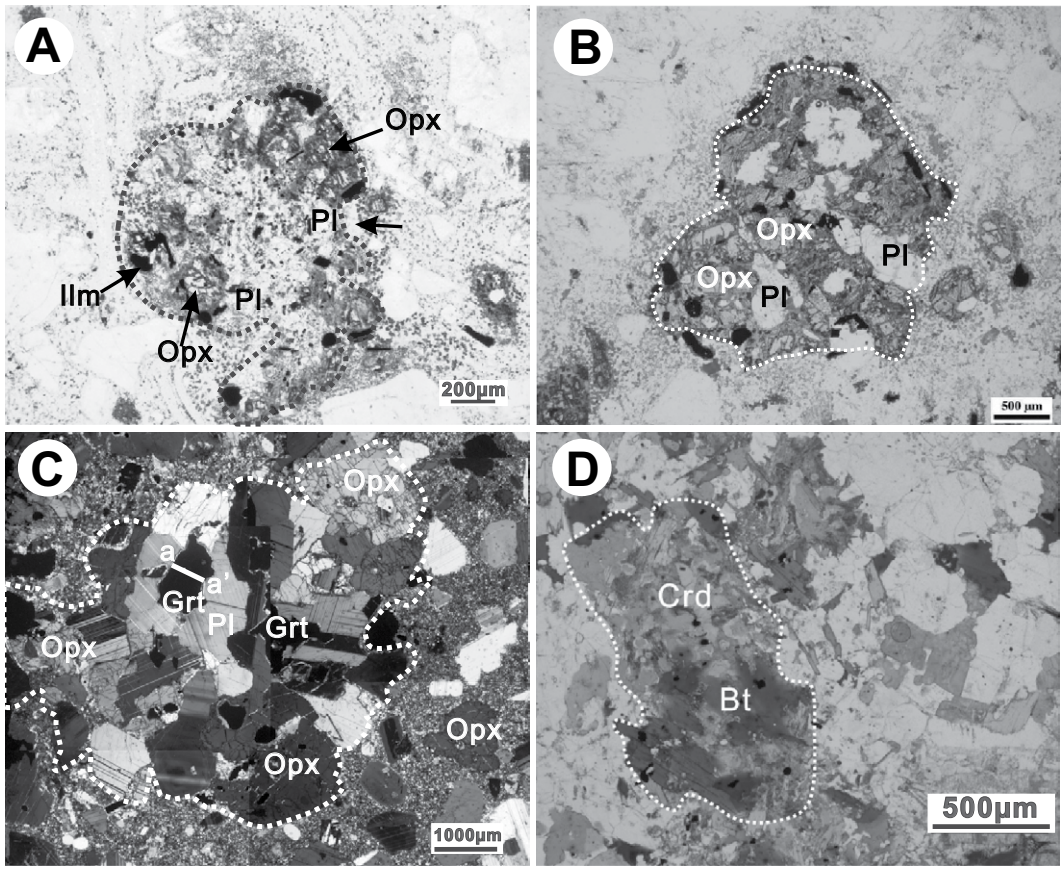

Figure 4. Mineral clusters hosted by the granitic rocks. (A–B) Mineral cluster of orthopyroxene (Opx) + plagioclase (Pl) + ilmenite (Ilm) from the (A) Taima pluton and (B) Dasi pluton. (C) Rare mineral cluster with garnet (Grt) + Opx + Pl from the Dasi pluton. (D) Rare cordierite-biotite (Crd-Bt) cluster with abundant sillimanite inclusions from the Jiuzhou pluton.

Zhao et al. (2012), except that quartz is only present as rare inclusions in plagioclase. The garnet in these crystal clusters has a relatively high pyrope content (23–26 wt%), showing increasing X_{Ca} and nearly constant X_{Mg} from core to rim (Fig. 3B). Orthopyroxene in the clusters has low X_{Mg} but high Al_2O_3 content (2.9–4.16 wt%), while the X_{An} of plagioclase is ~0.5.

The Jiuzhou granite has a medium- to coarse-grained equigranular texture (Fig. 2F), and it was thus likely emplaced at a deeper level than the Taima-Dasi pluton. The Jiuzhou granite consists of plagioclase (30–53 vol%), quartz (25–35 vol%), alkali feldspar (10–30 vol%), biotite (~8 vol%), orthopyroxene (~5 vol%), and cordierite (<1 vol%), and accessory minerals including zircon, monazite, apatite, and ilmenite. Orthopyroxene forms euhedral single crystals or clusters of ≤2–3 crystals. The orthopyroxene crystals have sizes of 0.4–2 mm (Fig. 2F), and they are typically inclusion-free or contain few ilmenite but no plagioclase inclusions. They differ in size and shape from orthopyroxene in the Grt-rich and Pl-poor granulite enclaves (where orthopyroxene forms fine-grained symplectite with cordierite; Fig. 2B) and from orthopyroxene in the Opx- and Pl-rich granulite enclaves (where orthopyroxene has anhedral shape and ilmenite inclusions). The euhedral orthopyroxene single crystals also have comparatively low X_{Mg} (X_{Mg} = 0.36–0.47) and low Al_2O_3 content (~0.5–1.0 wt%; Fig. 3A). Cordierite crystals are locally present as subhedral-euhedral inclusions in orthopyroxene and plagioclase, which are altered to fine-grained sericite and chlorite. Anhedral cordierite with biotite and sillimanite also forms clusters up to ~3 mm in dimension (Fig. 4D). The mineral assemblage of the clusters is comparable to that of the matrix assemblage of the Grt-rich and Pl-poor granulite enclaves (Fig. 2C).

ANALYTICAL RESULTS

Whole-Rock Major-Element and Trace-Element Compositions

All samples from the Jiuzhou, Dasi, and Taima plutons have moderately to strongly peraluminous composition (A/CNK = 1.07–1.12, 1.09–1.12, and 1.11–1.40, respectively, where A/CNK = $Al_2O_3/[CaO + Na_2O + K_2O]$; Table 4). The SiO_2 content of the Dasi and Taima plutons is high, and they show minor variation (69–70 wt% and 71–74 wt%, respectively; Table 4). The Al_2O_3 content of both plutons is comparable (14–16 wt%), whereas the Fe_2O_3 and CaO contents are slightly lower, and the K_2O content is slightly higher for the Taima compared to the Dasi granitic rocks (Fig. 5C). The SiO_2 content of the Jiuzhou pluton shows a relatively large variation (63–70 wt%), trending from low SiO_2 to SiO_2 values that overlap with those of the Dasi and Taima plutons (Fig. 5). Al_2O_3, Fe_2O_3, and CaO contents decrease and K_2O content increases with decreasing SiO_2, where all sample compositions overlap with those of the Dasi pluton. Compared to the granitic samples, the granulite enclaves have (1) lower SiO_2 content, i.e., ~45, 49, and 56 wt%; (2) higher Al_2O_3 and Fe_2O_3 contents (Figs. 5A and 5B); (3) equivalent or lower K_2O contents (Fig. 5C); and (4) lower or higher CaO contents (Fig. 5D).

The granulite enclaves and their granite hosts have comparable rare earth element (REE) distribution patterns, but they differ in REE content (Fig. 5E). They are all enriched in light (L) REEs and depleted in heavy (H) REEs, and they show a negative Eu anomaly (Eu/Eu* = 0.38–0.61). The Jiuzhou pluton shows relatively large variations in total REE content (310–180 ppm), while the REE content of the samples from the Taima and Dasi plutons is generally low and less variable (~220–240 ppm and 190–210 ppm, respectively). The total REE content of the granulite enclaves (~230–360 ppm) is, however, higher than that of the granitic samples (~180–310 ppm).

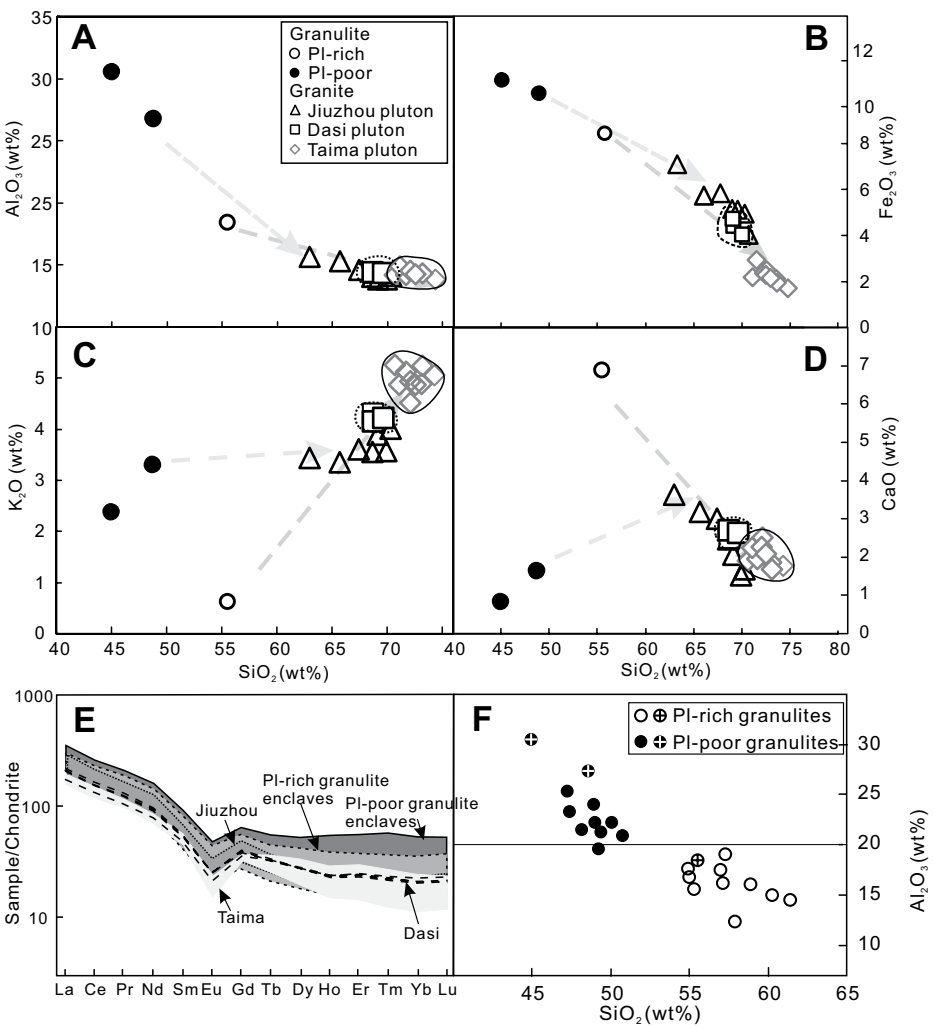

Figure 5. (A–D) Al_2O_3, Fe_2O_3, K_2O, and CaO vs. SiO_2 compositions of granulite enclaves and their host granite. Different compositional variation trends for the Taima-Dasi and the Jiuzhou plutons and their enclaves are indicated by the dashed arrows. Pl—plagioclase. (E) Rare earth element (REE) patterns for enclaves and granite. (F) SiO_2 vs. Al_2O_3 diagram showing the chemical difference between the orthopyroxene- and Pl-rich and the garnet-rich and Pl-poor enclaves. Compositional data for the enclaves in D and E are from Zhao et al. (2012) (filled and empty symbols) and from this study (symbols marked by a cross).

Whole-Rock Sr-Nd Isotopic Composition

The granite samples have high $^{86}Sr/^{87}Sr_i$ values, ranging from 0.71874 to 0.72157, and they have low $\varepsilon_{Nd}(t)$ values, ranging from –11.2 to –11.6, a signature which is commonly interpreted to suggest a source from recycled crustal sediments (e.g., Qi et al., 2007). Compared with the granite, the granulite enclaves show a significantly larger range of $^{86}Sr/^{87}Sr_i$ values (0.72636–0.74020) and predominantly lower $\varepsilon_{Nd}(t)$ values (–12.7 to –15.1; Fig. 6A).

Zircon U-Pb Ages and Hf Isotopic Composition

Four samples, one from the Taima (TM03), one from the Dasi (DS04-1), and two from the Jiuzhou pluton (JZ03-4 and JZ09), were selected for zircon U-Pb dating and Hf isotopic analysis. All data are shown in the supplementary Tables DR2 and DR3, Figures DR3 and DR4, and in Figure 7 (see footnote 1 for DR files). Zircon from the selected samples is predominantly short to long prismatic in shape, showing well-developed oscillatory zoning. Fifteen U-Pb analyses on zircon from the Taima pluton (sample TM03) yielded a weighted mean $^{206}Pb/^{238}U$ age of 255 ± 1.9 Ma (mean square of weighted deviates [MSWD] = 0.27; for supporting information, see Table DR2 and Figure DR3 [see footnote 1]); 13 analyses on zircon from the Dasi pluton (sample DS04-1) yielded an age of 249 ± 2.1 Ma (MSWD = 0.42); 18 and 17 analyses on zircon from two samples from the Jiuzhou pluton (samples JZ03-4 and JZ09) yielded ages of 245 ± 2.1 Ma (MSWD = 0.23) and 246 ± 2.3 Ma (MSWD = 0.19), respectively (Fig. DR3 [see footnote 1]). The Taima and Dasi plutons are thus slightly older (255–249 ± 2 Ma) than the Jiuzhou pluton (245–246 ± 2 Ma). Zircon crystals from the three granite plutons show comparable values but large ranges in Hf isotopic compositions, with $\varepsilon_{Hf}(t)$ values between –2.7 and –15.2 for the Taima pluton, between –1.9 and –11.9 for the Dasi pluton, and between –5.7 and –14.1 for the Jiuzhou pluton (Fig. 7). Data from Zhao et al. (2010) for zircon from granulite enclaves from the Jiuzhou pluton closely compare to those of the granitic zircon ($\varepsilon_{Hf}[t]$ ~–7 to –16), but they appear to lack $\varepsilon_{Hf}(t)$ values ≥–6.

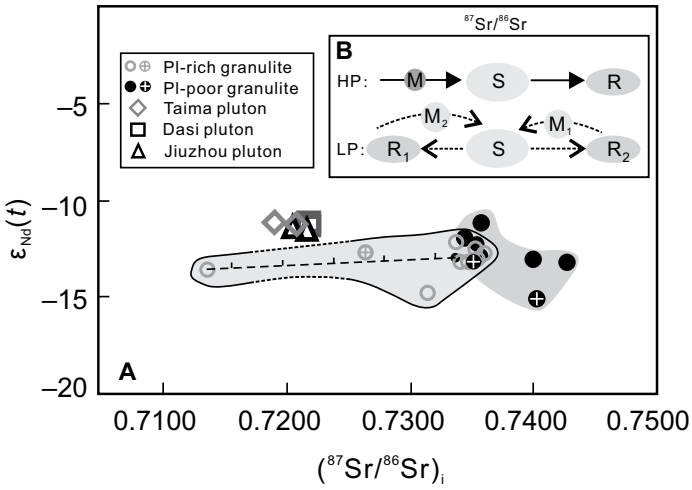

Figure 6. (A) $\varepsilon_{Nd}(t)$ vs. initial $^{87}Sr/^{86}Sr$ composition of granulite enclaves and their host granite. Filled and empty symbols are data from Zhao et al. (2012); data marked by a cross are from this study. Data for sample 06QZ-35-1 from Zhao et al. (2012), with a high Rb content (456 ppm) and Rb/Sr ratio (13.23), are not reported. Pl—plagioclase. (B) Schematic diagram indicating variations in Sr isotopic composition between the unmelted source (S) and restite (R)–melt (M) pairs inferred for the low-pressure (LP) and high-pressure (HP) melting events recorded by the orthopyroxene- and plagioclase-rich and the garnet-rich and plagioclase-poor enclaves, respectively. R_1 and R_2 represent possible Sr isotopic composition for restite produced at low (R_1) and high (R_2) degrees of partial melting.

PHASE EQUILIBRIUM MODELING

The *P-T* crystallization conditions for the granulite enclaves were quantitatively investigated by *P-T* pseudosection modeling. The *P-T* pseudosections were calculated with the Perple_X computer program package (Connolly, 2005; version from 6.7.0) and the internally consistent thermodynamic data set of Holland and Powell (1998, updated 2002). The following activity-solution models were used in the pseudosection calculations: Holland and Powell (1998) for garnet, Holland and Powell (1996) for orthopyroxene, Tajčmanová et al. (2009) for biotite, ideal models for cordierite, ilmenite, and sillimanite, Fuhrman and Lindsley (1988) for plagioclase, and White et al. (2001) for melt. The *P-T* pseudosections were calculated for a range of temperatures (800–1000 °C) and pressures (100–900 MPa) in the model system $MnO\text{-}Na_2O\text{-}CaO\text{-}K_2O\text{-}FeO\text{-}MgO\text{-}Al_2O_3\text{-}SiO_2\text{-}H_2O\text{-}TiO_2$ (Mn-NCKFMASHT). The compositions employed in the calculations are those of sample DS04-2 for the Opx- and Pl-rich enclaves, and those of samples JZ01-2 and JZ02-3 for the Grt-rich and Pl-poor enclaves (Table 4).

To model the conditions of source partial melting using the bulk composition of restite enclaves and their mineral assemblage, the effect of contamination or reequilibration of the enclaves with the host magma should be considered. The three enclave samples selected for whole-rock geochemical analysis and *P-T* modeling showed no evidence for the injection of granitic microveins or rehydration reactions (Figs. DR1 and DR2 [see footnote 1]). This strongly suggests that contamination by melt derived from the granitic host magmas did not take place. The compositional change of some minerals in the enclaves affected by diffusive reequilibration during magma residence, however, needs to be considered. Garnets show only weak zoning, and orthopyroxene and plagioclase in the enclaves are homogeneous, highlighting that their compositions were not significantly affected by diffusive reequilibration during magma residence. Considering a garnet grain with a diameter of ~1 mm and with MgO and FeO contents of ~4.7 wt% and ~31.5 wt%, respectively, a decreases in MgO content to ~4.1 wt% and a concomitant increase in FeO content to ~32.2 wt% within the outer ~100 μm of the crystal will shift the bulk composition of the crystal to ~4.5 wt% MgO and ~31.7 wt% FeO, i.e., a change on the order of <5%, which is within the error of analysis. Ilmenite is a phase that is more easily affected by reequilibration during system cooling than garnet, orthopyroxene, and plagioclase, because diffusion in ilmenite is fast (on the order of 10^{-13} to 10^{-16} m^2/s vs. 10^{-18} to 10^{-20} m^2/s for garnet at 1000 °C; e.g., Stenhouse et al., 2010; Carlson, 2006). For ilmenite, Mn and Fe-Mg diffusion is significantly faster than the diffusion of Ti and Al (Stenhouse et al., 2010).

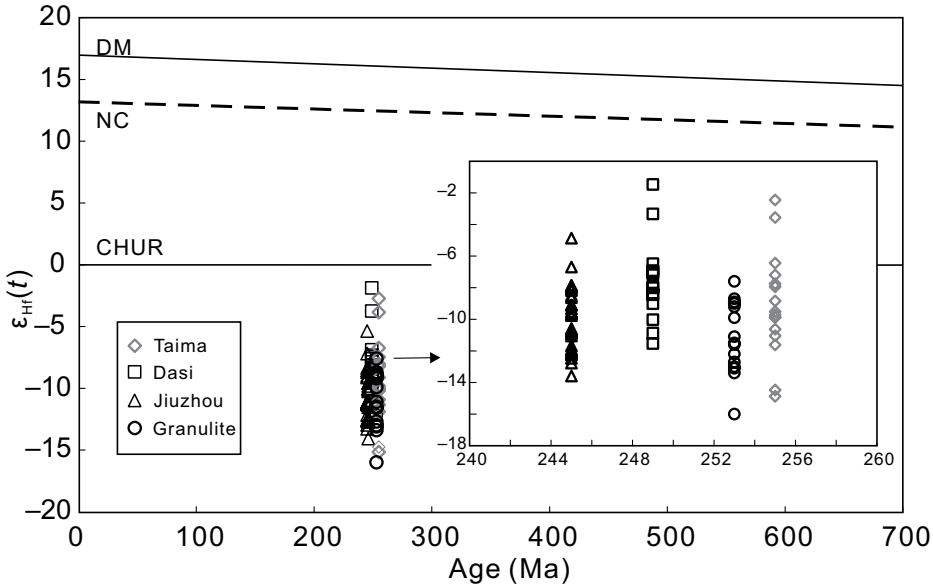

Figure 7. Zircon U-Pb ages and Hf isotopic compositions for granulite enclaves (Zhao et al., 2010) and their granite hosts, which are nearly identical in absolute values and in range. CHUR—chondritic uniform reservoir; NC—new continental crust; DM—depleted mantle.

A change in ilmenite X_{Mg} and Ti and Al content should have, in any case, a minor effect on the enclave composition, because the enclave Fe-Mg, Ti, and Al contents are largely controlled by garnet, orthopyroxene, and plagioclase, and these phases are only weakly zoned or homogeneous. The change in ilmenite MnO content toward higher MnO with cooling may, however, have significantly affected the MnO content if ilmenite was the major carrier of MnO.

A change in system MnO content, in turn, significantly affects the garnet stability field (Mahar et al., 1997; López-Carmona et al., 2010; Zhao et al., 2017). Experimental study (Green, 1977) suggests that an increase in MnO content (in a modal pelitic composition with ~64.5 wt% SiO_2) by ~0.2 wt% stabilizes the garnet stability field toward lower pressure by ~100 MPa and to lower temperature by >20 °C. The high ilmenite Mn content of ~3.8 wt% in the Opx- and Pl-rich enclaves and ~1.9 wt% in the Grt-rich and Pl-poor enclaves is characteristic for reequilibration at ≤750 °C (e.g., Hildreth, 1979), while the initial ilmenite MnO content can be estimated to have been ≤1 wt% for both enclaves at temperatures of >800 °C (cf. Hildreth, 1979). The system MnO content is thus considered to have been as low as 0.03–0.06 wt% compared to the preserved 0.10 wt% for the Opx- and Pl-rich enclaves and 0.06–0.12 wt% for the Grt-rich and Pl-poor enclaves, respectively. To assess the effect of partial Mn reequilibration of the enclaves on the *P-T* condition estimates, modeling using both the original and the corrected MnO contents was carried out.

The whole-rock composition of the granulite enclaves is melt-depleted, and for the purpose of modeling these restitic compositions, we followed the method of Taylor et al. (2014) and Nicoli et al. (2015). The preservation of the dry, granulite-facies assemblages in the enclaves is a consequence of melt loss at or shortly prior to peak metamorphic conditions (e.g., White and Powell, 2002). The melt remaining in the rock should be less than 20 vol% for an aluminous metapelitic system, or the peak metamorphic assemblage will undergo complete retrogression (White and Powell, 2002). For a granulitic rock in which the peak metamorphic assemblage is largely preserved, the unextracted melt in the rocks should be <5–10 vol% (cf. Taylor et al., 2014; Nicoli et al., 2015). The H_2O contents in the modeled systems were constrained to values at which an unextracted melt modal abundance of 5–10 vol% is predicted in equilibrium with the peak metamorphic assemblage and mineral abundance (Figs. 8A, 8C, and 9A; cf. Taylor et al., 2014; Nicoli et al., 2015). Following this method, the phase equilibrium of the peak metamorphic assemblage and part of the high-*T* retrograde path after melt loss from the system can be modeled (Nicoli et al., 2015).

P-T-XH_2O Modeling for the Grt-Rich and Pl-Poor Enclaves from the Jiuzhou Pluton

For the Grt-rich and Pl-poor granulite enclaves (samples JZ01-2 and JZ02-3), the peak metamorphic assemblage is dominated by subhedral to anhedral garnet porphyroblasts and single, anhedral cordierite crystals. Alkali feldspar (Kfs), biotite (Bt), and rare plagioclase (Pl) are present as inclusions in garnet (Grt) and cordierite (Crd), or they form single crystals between cordierite and garnet. Sillimanite (Sil) forms abundant inclusions in garnet and cordierite. Quartz (Qtz) should not have been present in the peak metamorphic assemblage, since spinel (Spl) was produced during the retrograde stage, which indicates that the system was silica-undersaturated. The peak metamorphic assemblage is thus inferred to have been Grt + Sil + Crd + Bt + Pl + Kfs + ilmenite (Ilm) + melt.

T-XH_2O pseudosections were iteratively modeled at variable pressures to constrain these parameters in the bulk composition to values consistent with the formation of the observed peak metamorphic assemblage. Figures 8A and 8C constrain the peak metamorphic assemblage to a H_2O content of 0.4–1.0 wt% at ~700 MPa. Considering nearly complete melt loss during the peak metamorphic stage (on the basis of the nearly complete preservation of the peak metamorphic assemblage), the melt isopleths (<5–10 vol%; cf. Taylor et al., 2014; Nicoli et al., 2015) further constrain the system H_2O content to 0.4–0.6 wt% (Fig. 8A) and 0.4 wt% (Fig. 8C) for the two modeled samples. In the following, *P-T* pseudosections were constructed at a system H_2O content of 0.4 wt%. If the system H_2O content was higher, e.g., 0.5 wt%, then the calculated temperature would be ~10 °C lower. A change in system MnO content by reequilibration was also considered, but the phase stability fields using corrected lower bulk-rock MnO content (i.e., ~0.03 and ~0.05 wt% instead of 0.06 and 0.12 wt% for JZ01-2 and JZ02-3, respectively) are not different from those using the bulk-rock MnO content. The effect of compositional reequilibration thus exerted little control on the *P-T* modeling results for the Grt-rich and Pl-poor enclaves. This may be because the dominant phase that controls MnO content in the Grt-rich and Pl-poor enclaves is garnet instead of ilmenite, and garnet is only weakly zoned.

The *P-T* pseudosections calculated for a system H_2O content of 0.4 wt% constrain the peak metamorphic conditions to 890–940 °C and 660–700 MPa for sample JZ01-2 (Fig. 8B), and to 860–920 °C and 640–710 MPa for sample JZ02-3 (Fig. 8D). The estimated conditions for the two samples overlap at 890–920 °C and 660–710 MPa. The *P-T* pseudosections also provide constraints on the retrograde path for the two samples (Figs. 8B and 8D), where the retrograde metamorphic assemblage is considered to have formed through reaction of the peak metamorphic assemblage with unextracted melt (evidence for melt-melt or melt-solid reaction between enclaves and their host magma in the

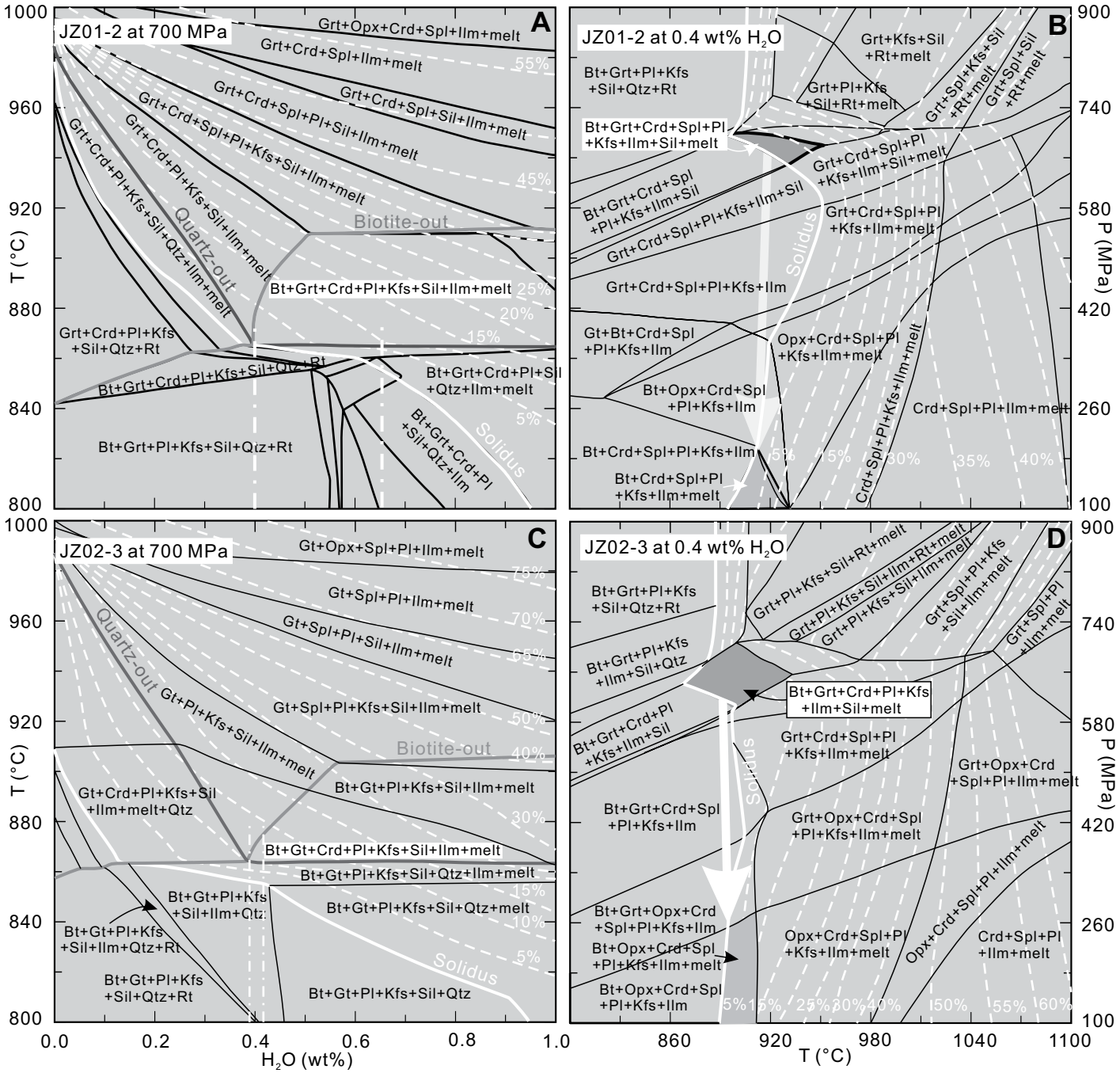

Figure 8. (A, C) Temperature-composition (T-$X\mathrm{H_2O}$) and (B, D) pressure-temperature (P-T) pseudosections calculated using the composition of the garnet-rich and plagioclase-poor granulite enclaves (A and B for JZ01-2; c and d for JZ02-3) for the system Mn-NCKFMASHT using Perple_X. The thick solid white lines indicate the solidus. The labeled white dashed lines indicate isopleths of melt volume fraction. The dark-gray areas in B and D indicate the stability fields corresponding to peak and retrograde metamorphic assemblages. The white arrows indicate the P-T paths during retrograde metamorphism. The dot-dashed white lines in A and C indicate the inferred variation in the H_2O content. The mineral assemblages of unlabeled fields can be found in Figure DR5 (see text footnote 1). Mineral abbreviations are those of Whitney and Evans (2010).

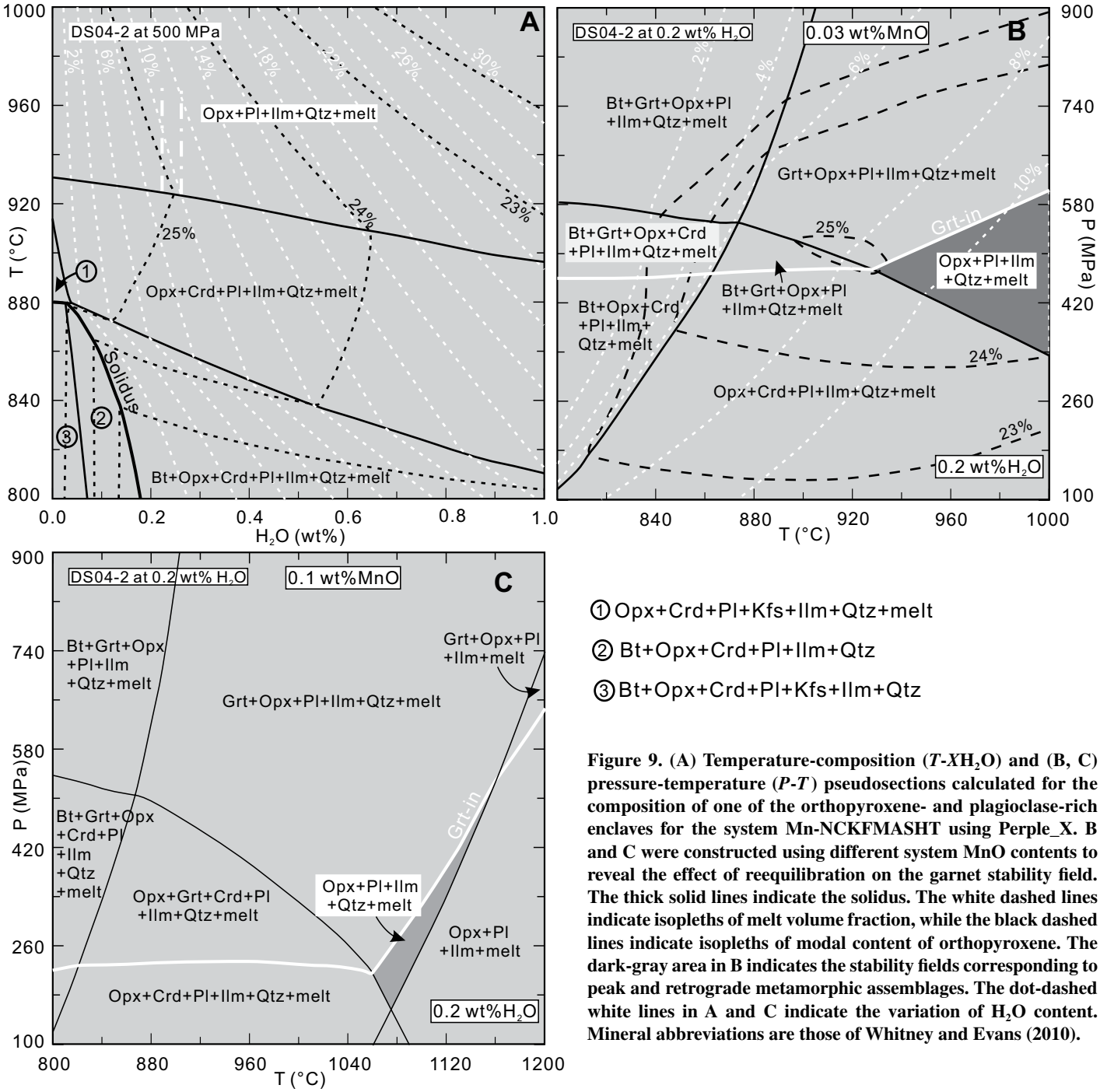

Figure 9. (A) Temperature-composition (*T*-*X*H_2O) and (B, C) pressure-temperature (*P*-*T*) pseudosections calculated for the composition of one of the orthopyroxene- and plagioclase-rich enclaves for the system Mn-NCKFMASHT using Perple_X. B and C were constructed using different system MnO contents to reveal the effect of reequilibration on the garnet stability field. The thick solid lines indicate the solidus. The white dashed lines indicate isopleths of melt volume fraction, while the black dashed lines indicate isopleths of modal content of orthopyroxene. The dark-gray area in B indicates the stability fields corresponding to peak and retrograde metamorphic assemblages. The dot-dashed white lines in A and C indicate the variation of H_2O content. Mineral abbreviations are those of Whitney and Evans (2010).

form of textural and/or mineralogical/compositional enclave core-rim zoning is lacking). For sample JZ01-2, the retrograde metamorphic assemblage of Crd + Spl + Bt + Pl + Kfs + Ilm suggests that the granulite partially reequilibrated at 890–920 °C and 100–260 MPa. The retrograde metamorphic assemblage of Opx + Crd + Spl + Bt + Pl + Kfs + Ilm in sample JZ02-3 is different from that of sample JZ01-2, in which orthopyroxene is present, which is in accordance with the higher enclave bulk SiO_2 content. The calculated conditions of partial reequilibration are constrained to 890–920 °C and 100–260 MPa.

P-T-XH_2O Modeling for the Opx- and Pl-Rich Enclaves from the Dasi Pluton

The characteristic mineral assemblage of the Opx- and Pl-rich granulite enclaves (sample DS04-2) is Opx + Pl + Qtz + Ilm. Clinopyroxene is locally present in DS04-2 (<1 vol%), where it forms round crystals around biotite inclusions, but it is not predicted in the pseudosection modeling. Previous studies have shown that clinopyroxene may form by biotite dehydration in the absence of Al_2SiO_5 at 870–880 °C (at 500–1000 MPa; Clemens and Vielzeuf, 1987), and we suggest that clinopyroxene in our samples formed in such a reaction. Its presence in the enclaves thus likely represents partial disequilibrium, i.e.,

partial preservation of the prograde metamorphic assemblage. Another possibility is that the lack of clinopyroxene in the modeled phase stability field reflects uncertainties of the method, for example, in the activity models, which do not always accurately predict the stability of minor constituents (cf. Jiao et al., 2013). Contrary to the Grt-rich and Pl-poor restite of the Jiuzhou pluton, the Opx- and Pl-rich enclaves of the Dasi pluton do not show a record of retrograde metamorphism. The peak metamorphic assemblage is entirely preserved due to nearly complete melt loss and quenching of the magmas at temperatures of ~780 °C (Zhao et al., 2017).

In the *T*-XH_2O pseudosection, the system H_2O content was determined to be <0.2–0.3 wt%, using an estimated unextracted melt proportion of <10 vol% and an orthopyroxene abundance of ~25 vol% (Fig. 9A). In the following, the *P-T* pseudosection was constructed at a system H_2O content of 0.2 wt%. If the system H_2O content was lower by 0.1 wt%, then the calculated temperature would increase by ~10 °C. The system MnO content is moreover anticipated to significantly affect the *P-T* model estimates (Figs. 9B and 9C). The stability field of garnet in the model system using measured bulk-rock MnO content extends to pressures as low as ~200 MPa and temperatures up to >1040–1200 °C (Fig. 9C), which are high and likely represent an overestimation compared to experimental findings (e.g., Patiño-Douce and Beard, 1996). As noted already, this is caused by the change in the system composition during reequilibration of ilmenite. In the following, a corrected system MnO content of ~0.03 wt% (instead of 0.1 wt%) was used in the modeling. The metamorphic assemblage of Opx + Pl + Ilm + Qtz + melt, an estimated unextracted melt volume of 5%–10%, and an orthopyroxene modal abundance of ~25% (Fig. 9B) constrain the peak metamorphic conditions to 920–980 °C and 420–580 MPa, i.e., 950 ± 30 °C and 500 ± 80 MPa (Fig. 9B).

DISCUSSION

Restitic Origin of the Granulite Enclaves and Link with their Granitic Host Rocks

Enclaves in granite may have a variety of origins. They may represent cognate cumulates (Phillips et al., 1981), mafic microgranular enclaves derived from magma mixing (Holden et al., 1987; Vernon, 2014), restite (Chappell et al., 1987), or xenoliths (Wall et al., 1987). The studied enclaves contain diagnostic metamorphic minerals, i.e., garnet, cordierite, orthopyroxene, and spinel, which show metamorphic textures, ruling out a cognate cumulate or microgranular enclave origin. Compared with metasedimentary rocks exposed in the nearby Yunkai terrane (Fig. 10A; Qiao et al., 2015; Wan et al., 2010) and compared with a typical metapelite composition (the North American shale; Fig. 10B), the granulite enclaves are rich in Al_2O_3, FeO, MgO, TiO_2, REE, and transitional elements, and they are depleted in SiO_2, Na_2O, K_2O, and Rb, which are characteristic for melt-depleted, residual material (cf. Sawyer et al., 2011). The enclaves thus have a high-grade metamorphic origin, but they could represent restitic fragments entrained from the source or host-rock xenoliths entrained by the granitic magma during ascent or at the emplacement level.

Zircon in the granitic rocks of the Taima, Dasi, and Jiuzhou plutons has Hf isotopic compositions comparable to zircon of the granulite enclaves reported by Zhao et al. (2012) (Fig. 7). Zircon U-Pb ages for granulite metamorphism are 253 ± 5 Ma (Zhao et al., 2010) and 248 ± 3 Ma (Jiao et al., 2015), and they are thus equivalent within error to the crystallization ages of 255 ± 2 Ma and 246 ± 2 Ma that were determined for the Taima, Dasi, and Jiuzhou plutons, respectively (Fig. DR2 [see footnote 1]). It is therefore concluded that the equivalent ages (within the uncertainty of the method) of the two types of granulite enclaves, with their corresponding host granitic rocks, suggest that the granulite enclaves are restite from the magma source and not host-rock xenoliths of younger crustal strata.

The crystal clusters of Opx-Pl-Ilm in the Taima-Dasi pluton and the Crd-Bt-Sil crystal clusters in the Jiuzhou pluton (Fig. 4) have the same assemblage, mineral composition, and mineral textures as the obvious centimeter- to decimeter-scale Opx- and Pl-rich enclaves and the Grt-rich and Pl-poor enclaves, respectively (Fig. 2), and they are thus interpreted as microrestite. These microrestites may have influenced the compositional variation of the granitic rocks. The way in which the presence of the microrestite fragments has influenced the compositional variation of the granitic rocks was evaluated using compositional variation in Fe, Mg, Ti, Ca, Na, and K (Fig. 11). The compositional variation of the Jiuzhou granite reflects fractional crystallization of an Opx-Pl-Ilm assemblage (Opx forms magmatic crystals in the Jiuzhou granite, as suggested by its euhedral shape and its X_{Al}-poor composition, which is distinct from enclave orthopyroxene; Fig. 2B vs. Figs. 2F and 3A), but it indicates that entrainment of microrestitic Grt, Crd, Bt, and Sil played

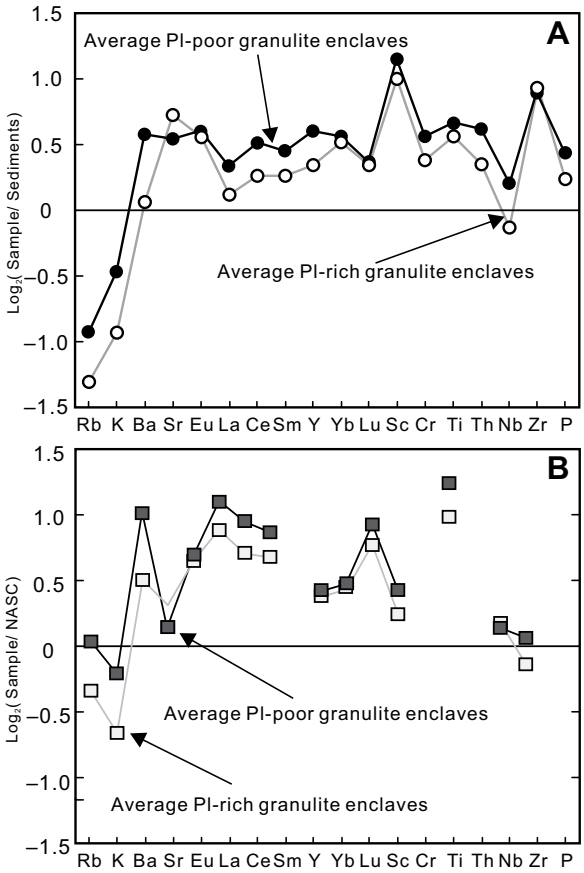

Figure 10. Average trace-element concentrations for the two groups of granulite enclaves normalized to the composition of possible metasedimentary source rocks from the Yunkai group (Wan et al., 2010; Qiao et al., 2015) and typical North American shale composition (NASC; Gromet et al., 1984). Pl—plagioclase.

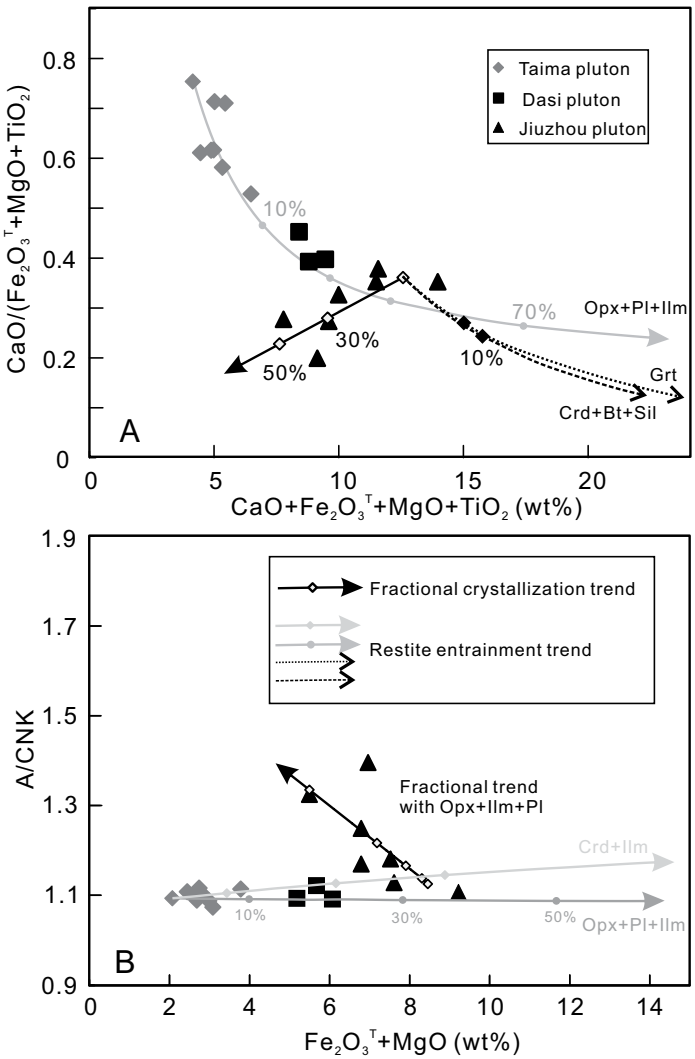

Figure 11. (A) $CaO/(Fe_2O_3^T + MgO + TiO_2)$ vs. $CaO + Fe_2O_3^T + MgO + TiO_2$ diagram. (B) A/CNK vs. $Fe_2O_3^T + MgO$ diagram, where $A/CNK = Al_2O_3/(CaO + Na_2O + K_2O)$. The compositional variation of the Taima-Dasi pluton complies with a restite entrainment trend, while fractional crystallization plays a more important role in the compositional variation of the Jiuzhou granite. The volume fraction for the indicated restite entrainment and fractional crystallization trends are 33% orthopyroxene (Opx) + 57% plagioclase (Pl) + 10% ilmenite (Ilm), and 15% Opx + 79% Pl + 6% Ilm, respectively. The compositions of garnet (Grt), Opx, and Pl correspond to compositions reported in Tables 1–3. Crd—cordierite; Bt—biotite; Sil—sillimanite.

only a minor role (Fig. 11A). This is consistent with the observation that microrestite is rare in our Jiuzhou granite sample suite. The Taima and Dasi whole-rock compositions follow a trend of restite entrainment from the most SiO_2-rich to the most SiO_2-poor samples, concurring with the relative abundance of microrestite in the samples (i.e., up to ~10 vol%; Figs. 4B, 4C, and 11). Comparing the geochemical composition of the granulite restites and the corresponding granitic melts/host rocks, it is further worth noting that (1) the Opx- and Pl-rich enclaves are relatively CaO-rich, yet they are hosted by the relatively CaO-poor Taima and Dasi plutons; and (2) the Grt-rich and Pl-poor enclaves are relatively CaO-poor, yet they are hosted by the relatively CaO-rich Jiuzhou pluton (Fig. 5D). This is unlikely to be coincidence, but it reflects the cognate link between the enclaves and their host magmas. The Taima and Dasi magmas share the same type of restite and similar mineral assemblages and textural features, and so the Taima and Dasi plutons are therefore hereafter termed the Taima-Dasi pluton.

Melting *P-T* Constraints for the Qinzhou Bay Granitic Complex

The pseudosection analysis of the Grt-rich and Pl-poor enclaves indicates source partial melting at ~905 ± 15 °C and ~675 ± 25 MPa. The inferred melting conditions are consistent with conditions inferred for other reported lower-crustal granulite enclaves (e.g., 850–950 °C and 700–1100 MPa for granulite enclaves from central Spain; Villaseca et al., 1999). The presence of biotite in the metamorphic assemblage suggests melting temperatures of <~920 °C at ~700 MPa (Vielzeuf and Montel, 1994). The presence of spinel in the Grt-rich and Pl-poor enclaves during retrograde metamorphism suggests that the system was SiO_2-undersaturated. Our inferred temperature estimate for the Grt-rich and Pl-poor enclaves is slightly higher, while the pressure estimate is slightly lower than previous estimates by Jiao et al. (2013), which suggested partial melting at 800–830 °C and 720–800 MPa. Possible interpretation for the lower temperature estimated by Jiao et al. (2013) is that a higher water content was used in their modeling; i.e., the produced melts had a high H_2O activity (e.g., >0.8 vs. <~0.3 in our modeling).

For the Opx- and Pl-rich enclaves, the pseudosection analysis constrains the peak metamorphic temperature to ~950 ± 30 °C and the pressure to ~500 ± 80 MPa. The corresponding metamorphic assemblage lacks biotite, suggesting that the melting temperature exceeded the biotite stability field at >850–875 °C at ~500 MPa (Vielzeuf and Montel, 1994). Crystallization temperatures for the Grt + Opx + Pl crystal clusters from the Dasi pluton, which lack quartz except for minor inclusions in plagioclase, can be estimated with the Grt-Opx thermometer of Sen and Bhattacharya (1984). The calculated temperatures are ~910 °C and ~950 °C for a pressure range of 0.3–0.8 Ga. The crystal clusters thus formed at the same temperatures of 910–950 °C as the Opx- and Pl-rich enclaves. The garnet-bearing mineralogy of these crystal clusters compared to the predominant garnet-free, Opx- and Pl-rich enclaves may suggest derivation from a slightly more peraluminous source.

Two-Stage Partial Melting at Different Crustal Levels

The geochronological results have revealed two stages of partial melting in the Qinzhou Bay granitic complex, i.e., an early melting

event at 255–249 Ma that produced magmas of the Taima-Dasi subvolcanic rocks and the corresponding Opx- and Pl-rich restites, and a later melting event at 246–245 Ma that produced the magmas of the Jiuzhou pluton and the corresponding Grt-rich and Pl-poor restites. The Opx- and Pl-rich restite enclaves hosted by the Taima-Dasi rocks indicate that the magmas were produced by partial melting at relatively low pressure, i.e., ~500 ± 80 MPa, at a depth of ~18 km (calculated for an average crustal density of 2.7 g/cm^3). This pressure is lower than the pressure recorded by the peak metamorphic assemblage of the Grt-rich and Pl-poor enclaves that produced the Jiuzhou magmas at 246–245 Ma, i.e., estimated to be ~675 ± 25 MPa, corresponding to partial melting at a depth of ~25 km. The melting pressure estimates from the restites thus suggest that source partial melting that generated the Taima-Dasi magmas occurred at midcrustal levels, while the Jiuzhou magmas were derived from a source at a deeper crustal level.

The increasing melting pressure can be interpreted to the record of migration of the magma source in response to regional tectonic evolution. The bulk-rock Sr-Nd and zircon Hf isotopic compositions suggest that the Taima-Dasi and Jiuzhou magmas were derived from an isotopically comparable source, while the mineralogical character of the two types of restites suggests that the composition of the source of the Jiuzhou magmas was different from the source of the Taima-Dasi magmas. The restites of the Jiuzhou magmas contain abundant sillimanite as inclusions in garnet and cordierite, which is interpreted as an unreacted phase during melting. This suggests that the protolith of the Jiuzhou magmas also contained abundant sillimanite, and it is thus likely that it approached the composition of an aluminous metapelite source. Sillimanite is, however, absent from the Opx- and Pl-rich enclaves, and the enclaves are rich in plagioclase. The Taima-Dasi magmas are thus likely to have been derived from a less aluminous metagraywacke source. The Taima-Dasi and Jiuzhou magmas were thus derived from compositionally and mineralogically variable source rocks, but their source rocks may have been part of a sedimentary supergroup, e.g., a succession of metapsammitic to metapelitic rocks, explaining their comparable isotopic composition.

The migrating source of the Jiuzhou magmas was likely located above the Taima-Dasi magma source, consistent with burial of the crustal section between the first melting event that produced the Taima-Dasi pluton and the later melting event that produced the Jiuzhou pluton, which juxtaposed the subvolcanic Taima-Dasi system (crystallized at <100–200 MPa) and the later constructed Jiuzhou pluton (crystallized at 200–300 MPa; Zhao et al., 2017). An alternative interpretation for source partial melting at different crustal levels is that mantle-derived magmas were predominantly emplaced at midcrustal levels during early stage and at deeper-crustal levels during a late stage, and that they therefore caused crustal partial melting at two significantly different levels. The first basalts, however, usually pond at the mantle-crust boundary, and then differentiated basalts heat up and partially melt crustal rocks at deep- to midcrustal levels.

The proposed source migration is consistent with the known evolution of the regional tectonic setting. Jiao et al. (2015) and Li et al. (2016) attributed the generation of the granitic and volcanic rocks in the Qinzhou Bay granitic complex to anatexis of continental crust in a subduction setting. The sedimentary record of the Shiwandashan Basin (which is spatially associated with the studied plutons; Fig. 1) suggests a change of dynamic drivers from subduction to continent-continent collision in the Late Permian. The basin was then closed during the Early Triassic (251–245 Ma), which is consistent with the time of collision between the Indochina and South China blocks during the Indosinian orogeny (250–245 Ma; Carter et al., 2001; Liang and Li, 2005; Roger et al., 2007; Faure et al., 2014; Hu et al., 2014). Our geochronological data reveal two stages of partial melting events, at 255–249 Ma that produced the Taima-Dasi magmas, and at 246–245 Ma that produced the Jiuzhou magmas, corresponding to the periods of subduction and continent-continent collision, respectively. The source melting conditions for the Taima-Dasi magmas are inferred to have been ~950 ± 30 °C and ~500 ± 80 MPa, corresponding to a geothermal gradient of ~51 °C/km, which is typical in a subduction setting (Sakaguchi, 1996). The source melting conditions for the Jiuzhou system, in contrast, are ~905 ± 15 °C and ~675 ± 25 MPa, corresponding to a geothermal gradient of ~36 °C/km, which is consistent with gradients typical for continent-continent collision settings (Imayama et al., 2012). The migration of the magma source to a deeper level is thus considered to have been a response to a tectonic switch at ca. 249 Ma from subduction to continent-continent collision. It is worth noting that a similar timing for the transition from subduction to collision at ca. 248 Ma was also inferred for closure of the western part of the subduction-collision belt of the paleo-Tethys Ocean along the Jinshajiang–Ailaoshan–Song Ma suture (Zi et al., 2012).

The partial melting at two different crustal levels within a short time scale of 3–10 m.y. requires a rapid tectonic burial rate and short duration of melt formation and segregation. The inferred rapid source migration from a depth of 18 km to 25 km over a time scale of 3–10 m.y. from 249 Ma to 246–245 Ma suggests a burial rate of 0.07–0.23 cm yr^{-1}. A comparable burial rate of ~0.17 cm yr^{-1} has been estimated for anatectic metapelites of the Bandelierkop Formation in the Limpopo belt of South Africa, which were transported from a shallow crustal to lower-crustal level during continent-continent collision (Nicoli et al., 2015). Recent studies have also suggested that the duration of melt formation and segregation is short, i.e., on an order of a few hundred thousand years (Bea et al., 2007; Neogi et al., 2014).

Possible Origin of Isotopic Variation between Restite Enclaves and Host Granitic Rocks

Sources and their corresponding magmas have the same isotopic composition if equilibrium between them is established (e.g., Villaseca et al., 1999). The studied granulite enclaves and their host granitic rocks are inferred to represent restite and corresponding melt, while they differ in whole-rock Sr-Nd composition. Possible explanations for these differences in isotopic composition are as follows.

Contamination of the granitic magma by country rocks took place en route to or at the emplacement level of the magmas (e.g., Erdmann et al., 2009). Evidence for country-rock–derived microxenoliths that could have affected our whole-rock compositional analyses is, however, lacking. Moreover, if such xenoliths were assimilated, we would anticipate to have detected a range in whole-rock isotopic composition.

Mixing of two or more magma/melt batches may have taken place (e.g., Kemp et al., 2007). Evidence for magma mixing in the form of microgranular enclaves is, however, lacking. The higher average $\varepsilon_{Nd}(t)$ composition of the granitic rocks compared to the enclave samples and high $\varepsilon_{Hf}(t)$ detected for some of their zircon values (i.e., $\varepsilon_{Hf}[t]$ values >–7; Fig. 7) may reflect the input of minor amounts of juvenile, mantle-derived melt. Our reservation with this interpretation is that mixing of small volumes of basaltic magma into large volumes of granitic magma is physically unlikely (Laumonier et al., 2014). Mixing by diffusion may have taken place, but this should have resulted in isotopically variable compositions for granitic rocks, and it is overall unlikely to have had a significant effect, as it would require a large contact surface area. The isotopic variation should moreover follow a compositional trend from high $(^{87}Sr/^{86}Sr)_i$ and low $\varepsilon_{Nd}(t)$ toward low $(^{87}Sr/^{86}Sr)_i$ and high

$\varepsilon_{Nd}(t)$, which is not the case. Mixing of two or more batches of crustal melt (e.g., Zhao et al., 2012), in contrast, is physically possible, but the $\varepsilon_{Nd}(t)$ composition of the granulite enclaves is systematically lower than that of the granitic samples. If two crustal melt batches mixed, then only one of the sources is represented in our data set and in the data set of Zhao et al. (2012). It is also possible that two crustal sources with different $(^{87}Sr/^{86}Sr)_i$ but equivalent $\varepsilon_{Nd}(t)$ and minor amounts of juvenile mantle–derived melt mixed. In this case, the Taima-Dasi and the Jiuzhou granitic rocks should have relatively low $(^{87}Sr/^{86}Sr)_i$ and high $(^{87}Sr/^{86}Sr)_i$ source-inherited composition, respectively, which is not the case.

Melts with different isotopic composition can also be produced from a common source by nonmodal partial melting (disequilibrium partial melting; Zou, 1998, 2000; Knesel and Davidson, 2002; Zeng et al., 2005; Farina and Stevens, 2011, 2014). The whole-rock LREE element compositions of the Taima, Dasi, and Jiuzhou granitic samples point to disequilibrium partial melting. The rocks have low LREE contents compared to LREE contents predicted at saturation (LREE*; Fig. 12). We therefore now consider if disequilibrium as a result of nonmodal partial melting may account for the variable isotopic composition of the studied granulite enclaves and the homogeneous composition of their host granitic rocks.

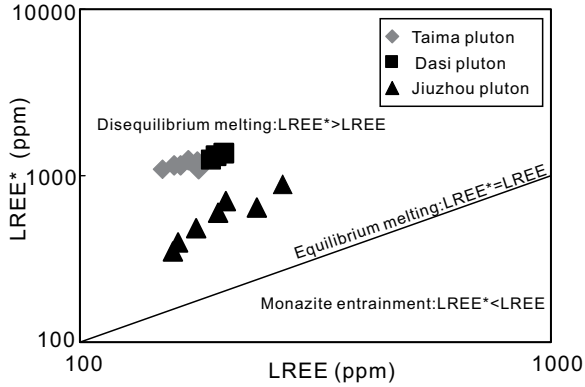

Figure 12. Calculated light rare earth elements (LREE*) vs. LREEs (observed) diagram (after Watt and Harley, 1993), where LREE* denotes the calculated LREE saturation concentration (cf. Watt and Harley, 1993). The temperatures used for the calculation were 950 °C for the Taima and Dasi plutons and 905 °C for the Jiuzhou pluton.

Sr Isotope Variation as a Result of Nonmodal Partial Melting

The Opx- and Pl-rich and the Grt-rich and Pl-poor restite enclaves show large variation in $(^{87}Sr/^{86}Sr)_i$, and their $(^{87}Sr/^{86}Sr)_i$ isotopic composition differs significantly from their granitic host rocks. In the following section, we calculate if and how nonmodal partial melting may have affected their Sr isotopic composition, following the approach of Zeng et al. (2005) and Farina and Stevens (2011). We first calculate nonmodal partial melting for the high-pressure case that produced the Grt-rich and Pl-poor restite. To calculate Sr and $^{87}Sr/^{86}Sr$ partitioning between restite and melt, we use a Sr content of 288 ppm and 30 ppm for biotite and plagioclase, respectively (cf. Zeng et al., 2005, and references therein), and the fraction of biotite and plagioclase consumed by experimental metagraywacke partial melting at 1000 MPa (the synthetic F-annite gneiss of Patiño-Douce and Beard, 1996; Fig. 13A). The amount of plagioclase consumed in the reaction increases from ~15 to >25 wt% at melting degrees of ~25 to ~55%, whereas the amount of biotite consumed in the reaction increases from ~10 wt% to >35 wt% at a melting degree of ~55% (Fig. 13A).

The Grt-rich and Pl-poor enclaves have low plagioclase content (< 3%), and biotite (~3 vol%) is thus the main Sr-bearing mineral. We therefore employ the Sr isotopic composition of one of the Grt- and Pl-poor enclaves (JZ01-1) with the lowest content of plagioclase as a proxy for the Sr isotopic composition of biotite in the source. The Sr isotopic composition of plagioclase in the source is unknown, and we therefore use a range of compositions to model the partitioning of $^{87}Sr/^{86}Sr$ between plagioclase and melt. The modeling results (Fig. 13B) indicate that the $^{87}Sr/^{86}Sr$ ratio of the partial melt generated by plagioclase-dominated partial melting is lower than that of the original source for relatively low degrees of melting (25%–45%). However, when the degree of partial melting is ≥45%, then the $^{87}Sr/^{86}Sr$ ratio of the melt approximates that of the unmelted metasedimentary source. For a high degree of melting near >45%–55%, which is inferred based on the high melting temperature, the Sr isotopic composition of the generated melt will therefore approximate that of the source.

In contrast to the Grt-rich and Pl-poor restite, the Opx- and Pl-rich restite has minor biotite (<3 vol%) but abundant plagioclase (up to ~50 vol%). Modeling the solid-melt partitioning of Sr and $^{87}Sr/^{86}Sr$ thus cannot assume that all Sr liberated in the melting reaction is released into the melt. At low melting degrees, a high amount of biotite will be consumed, which produces

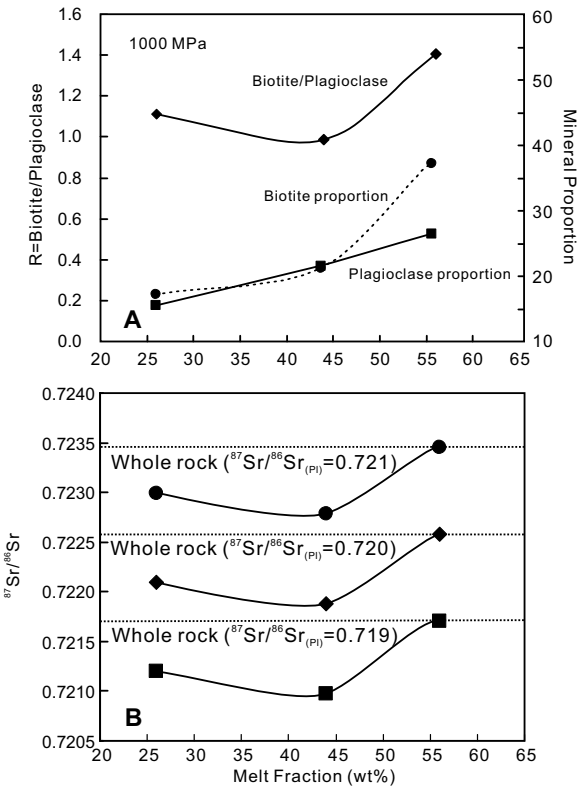

Figure 13. (A) Plot of estimated proportions in which biotite and plagioclase enter the melt (right-hand axis) and the ratio of these proportions (left-hand axis) at various melt fractions for high-pressure partial melting. The mineral proportions and melt fractions are those reported by Patiño-Douce and Beard (1996) for a metagraywacke that was partially melted at 1000 MPa and under dry conditions. (B) Estimation of the $^{87}Sr/^{86}Sr$ composition of the partial melt for biotite and plagioclase contributions as indicated in A and for a range of whole-rock Sr isotopic compositions (indicated by the dashed lines). Low-degree partial melt is predicted to have low $^{87}Sr/^{86}Sr$ composition compared to the unmelted source, while high-degree partial melt is predicted to have $^{87}Sr/^{86}Sr$ composition that approximates that of the unmelted source. Pl—plagioclase.

melt (M1) with a high $^{87}Sr/^{86}Sr$ composition and restite (R1) with a low $^{87}Sr/^{86}Sr$ composition (Hammouda et al., 1996; Fig. 6B). Experimental studies also suggest that the neoblastic, An-rich plagioclase (R2) formed by incongruent partial melting has a high $^{87}Sr/^{86}Sr$ composition compared to the reactant plagioclase and melt (M2; Fig. 6B; Hammouda et al., 1994, 1996).

Rapid magma production and extraction and dry partial melting conditions favor isotopic and/or elemental disequilibrium between source restite and melt (Knesel and Davidson, 1996, 2002). Hammouda et al. (1996) have suggested that total equilibration between melt and solid restite for $^{87}Sr/^{86}Sr$ takes ~10,000 yr to 1 m.y. (at 800–1000 °C and for crystal sizes of 0.1–1 cm). Sr isotopic disequilibrium between restite and coexisting partial melt is thus possible and even likely in zones of partial melting in both convergent orogens and in extensional settings, in which melt extraction is thought to take ~50,000–250,000 yr and up to ~10,000 yr, respectively (e.g., Bea et al., 2007; Neogi et al., 2014).

SUMMARY AND CONCLUSIONS

The studied restitic granulite enclaves and their host granitic rocks of the Taima-Dasi and Jiuzhou plutons in South China provide a wealth of information on their mid- to deep-crustal sources. Two populations of restitic enclaves, the Opx- and Pl-rich enclaves and the Grt-rich and Pl-poor enclaves, record two partial melting events: an early melting event at midcrustal levels at 255–249 Ma that involved an aluminum-poor metagraywacke source, and a later melting event at deep-crustal levels at 246–245 Ma that involved a comparatively aluminum-rich metapelitic source. The crustal source is thus inferred to have rapidly (within 3–10 m.y.) migrated from mid- to deep-crustal levels from ~18 to ~25 km, at burial rates of 0.07–0.23 cm yr^{-1}, in response to a switch in the geodynamic regime from subduction to continent-continental collision.

On the basis of the compositional variation of the studied Taima-Dasi and Jiuzhou plutons alone, it is inferred that their compositional variation may be affected by variable processes such as fractional crystallization and restite entrainment. However, combining restite-melt compositional and mineralogical data and their constraints on crystallization conditions and source allows us to resolve that the studied Taima-Dasi and Jiuzhou plutons were derived from sources that differed in location (depth), melting temperature, and rock type. Few upper-crustal intrusions carry components from their source regions that provide such detailed insights. We posit that the variations in source conditions that we have uncovered may also play an important role in other systems, especially for incrementally assembled large-scale intrusions.

ACKNOWLEDGMENTS

We are grateful to Z. Y. He and Z. L. Tian for introducing us to the details of the Perple_X software. We would like to sincerely thank Editors A. Cavosie and H. B. Zou for their helpful and constructive suggestions. We would also like to thank Y. J. Tang and other anonymous reviewers for their constructive comments on the manuscript. R. Klemd is also thanked for discussion and editorial comments for the previous version of the manuscript. This work was supported by the Natural Science Foundation of China (grant 41430208) and the National Basic Research Program of China (2012CB416701). All data relevant to this research have been included in the tables, in the supplementary files, or were taken from references published in the literature.

REFERENCES CITED

Acosta-Vigil, A., Buick, I., Hermann, J., Cesare, B., Rubatto, D., London, D., and Morgan, G.B., 2010, Mechanisms of crustal anatexis: A geochemical study of partially melted metapelitic enclaves and host dacite, SE Spain: Journal of Petrology, v. 51, no. 4, p. 785–821, doi:10.1093/petrology/egp095.

Bea, F., Montero, P., Gonzalez-Lodeiro, F., and Talavera, C., 2007, Zircon inheritance reveals exceptionally fast crustal magma generation processes in central Iberia during the Cambro-Ordovician: Journal of Petrology, v. 48, no. 12, p. 2327–2339, doi:10.1093/petrology/egm061.

Borgia, A., Tizzani, P., Solaro, G., Manzo, M., Casu, F., Luongo, G., Pepe, A., Berardino, P., Fornaro, G., Sansosti, E., Ricciardi, G.P., Fusi, N., Di Donna, G., and Lanari, R., 2005, Volcanic spreading of Vesuvius, a new paradigm for interpreting its volcanic activity: Geophysical Research Letters, v. 32, no. 3, L03303, doi:10.1029/2004GL022155.

Bureau of Geology Mineral Resource of Guangxi Zhuang Autonomous Region (BGMRGX), 1985, Reginal Geology of Guangxi Zhuang Autonomous Region: Beijing, Geological Publishing House, p. 429–445 (in Chinese).

Carlson, W.D., 2006, Rates of Fe, Mg, Mn, and Ca diffusion in garnet: The American Mineralogist, v. 91, no. 1, p. 1–11, doi:10.2138/am.2006.2043.

Carter, A., Roques, D., and Bristow, C., 2001, Understanding Mesozoic accretion in Southeast Asia: Significance of Triassic thermotectonism (Indosinian orogeny) in Vietnam: Geology, v. 29, no. 3, p. 211–214, doi:10.1130/0091-7613(2001)029<0211:UMAISA>2.0.CO;2.

Carvalho, P.C.S., Neiva, A.M.R., Silva, M.M.V.G., and Corfu, F., 2012, A unique sequential melting mechanism for the generation of anatectic granitic rocks from the Penafiel area, northern Portugal: Lithos, v. 155, p. 110–124, doi:10.1016/j.lithos.2012.08.019.

Chappell, B.W., White, A.J.R., and Wyborn, D., 1987, The importance of residual source material (restite) in granite petrogenesis: Journal of Petrology, v. 28, no. 6, p. 1111–1138, doi:10.1093/petrology/28.6.1111.

Chen, C.-H., Hsieh, P.-S., Lee, C.-Y., and Zhou, H.-W., 2011, Two episodes of the Indosinian thermal event on the South China block: Constraints from LA-ICPMS U-Pb zircon and electron microprobe monazite ages of the Darongshan S-type granitic suite: Gondwana Research, v. 19, no. 4, p. 1008–1023, doi:10.1016/j.gr.2010.10.009.

Clemens, J.D., and Droop, G.T.R., 1998, Fluids, *P-T* paths and the fates of anatectic melts in the Earth's crust: Lithos, v. 44, p. 21–36, doi:10.1016/S0024-4937(98)00020-6.

Clemens, J., and Vielzeuf, D., 1987, Constraints on melting and magma production in the crust: Earth and Planetary Science Letters, v. 86, p. 287–306.

Connolly, J.A.D., 2005, Computation of phase equilibria by linear programming: A tool for geodynamic modeling and its application to subduction zone decarbonation: Earth and Planetary Science Letters, v. 236, no. 1-2, p. 524–541, doi:10.1016/j.epsl.2005.04.033.

Erdmann, S., Jamieson, R.A., and MacDonald, M.A., 2009, Evaluating the origin of garnet, cordierite, and biotite in granitic rocks: A case study from the South Mountain Batholith, Nova Scotia: Journal of Petrology, v. 50, no. 8, p. 1477–1503, doi:10.1093/petrology/egp038.

Farina, F., and Stevens, G., 2011, Source controlled $^{87}Sr/^{86}Sr$ isotope variability in granitic magmas: The inevitable consequence of mineral-scale isotopic disequilibrium in the protolith: Lithos, v. 122, no. 3-4, p. 189–200, doi:10.1016/j.lithos.2011.01.001.

Farina, F., Dini, A., Rocchi, S., and Stevens, G., 2014, Extreme mineral-scale Sr isotope heterogeneity in granites by disequilibrium melting of the crust: Earth and Planetary Science Letters, v. 399, p. 103–115, doi:10.1016/j.epsl.2014.05.018.

Faure, M., Lepvrier, C., Nguyen, V.V., Vu, T.V., Lin, W., and Chen, Z., 2014, The South China block–Indochina collision: Where, when, and how?: Journal of Asian Earth Sciences, v. 79, p. 260–274, doi:10.1016/j.jseaes.2013.09.022.

Fuhrman, M.L., and Lindsley, D.H., 1988, Ternary-feldspar modeling and thermometry: The American Mineralogist, v. 73, p. 201–215.

Gerdes, A., 2001, Magma homogenization during anatexis, ascent and/or emplacement? Constraints from the Variscan Weinsberg granites: Terra Nova, v. 13, p. 305–312, doi:10.1046/j.1365-3121.2001.00365.x.

Green, T.H., 1977, Garnet in silicic liquids and its possible use as a *P-T* indicator: Contributions to Mineralogy and Petrology, v. 65, p. 59–67, doi:10.1007/BF00373571.

Gromet, L.P., Dymek, R.F., Haskin, L.A., and Korotev, R.L., 1984, The "North American shale composite": Its compilation, major and trace element characteristics: Geochimica et Cosmochimica Acta, v. 48, p. 2469–2482.

Hammouda, T., Pichavant, M., and Chaussidon, M., 1994, Mechanisms of isotopic equilibration during partial melting: An experimental test of the behaviour of Sr: Mineralogical Magazine, v. 58A, p. 368–369, doi:10.1180/minmag.1994.58A.1.193.

Hammouda, T., Pichavant, M., and Chaussidon, M., 1996, Isotopic equilibration during partial melting: An experimental test of the behaviour of Sr: Earth and Planetary Science Letters, v. 144, p. 109–121, doi:10.1016/0012-821X(96)00144-6.

Hildreth, W., 1979, The Bishop Tuff: Evidence for the origin of compositional zonation in silicic magma chambers, *in* Chapin, C.E., and Elston, W.E., eds., Ash-Flow Tuffs: Geological Society of America Special Paper 180, p. 43–76, doi:10.1130/SPE180-p43.

Holden, P., Halliday, A.N., and Stephens, W.E., 1987, Neodymium and strontium isotope content of microdiorite enclaves points to mantle input to granitoid production: Nature, v. 330, p. 53–56, doi:10.1038/330053a0.

Holland, T., and Powell, R., 1996, Thermodynamics of order-disorder in minerals: 2. Symmetric formalism applied to solid solutions: The American Mineralogist, v. 81, p. 1425–1437, doi:10.2138/am-1996-11-1215.

Holland, T., and Powell, R., 1998, An internally consistent thermodynamic data set for phases of petrological interest: Journal of Metamorphic Geology, v. 16, p. 309–343, doi:10.1111/j.1525-1314.1998.00140.x.

Holtz, F., and Barbey, P., 1991, Genesis of peraluminous granites II. Mineralogy and chemistry of the Tourem Complex (North Portugal). Sequential Melting vs. Restite unmixing: Journal of Petrology, v. 32, no. 5, p. 959–978.

Hu, L., Du, Y., Cawood, P.A., Xu, Y., Yu, W., Zhu, Y., and Yang, J., 2014, Drivers for late Paleozoic to early Mesozoic orogenesis in South China: Constraints from the sedimentary record: Tectonophysics, v. 618, p. 107–120, doi:10.1016/j.tecto.2014.01.037.

Imayama, T., Takeshita, T., Yi, K., Cho, D.-L., Kitajima, K., Tsutsumi, Y., Kayama, M., Nishido, H., Okumura, T., Yagi, K., Itaya, T., and Sano, Y., 2012, Two-stage partial melting and contrasting cooling history within the Higher Himalayan Crystalline Sequence in the far-eastern Nepal Himalaya: Lithos, v. 134–135, p. 1–22, doi:10.1016/j.lithos.2011.12.004.

Jiao, S.J., Guo, J.H., and Peng, S.B., 2013, Petrogenesis of garnet in the Darongshan-Shiwandashan granitic suite

of the South China block and the metamorphism of the granulite enclave: Acta Geologica Sinica, v. 29, no. 5, p. 1740–1758.

Jiao, S.-J., Li, X.-H., Huang, H.-Q., and Deng, X.-G., 2015, Metasedimentary melting in the formation of charnockite: Petrological and zircon U-Pb-Hf-O isotope evidence from the Darongshan S-type granitic complex in southern China: Lithos, v. 239, p. 217–233, doi:10.1016/j.lithos.2015.10.004.

Kemp, A.I.S., Hawkesworth, C.J., Foster, G.L., Paterson, B.A., Woodhead, J.D., Hergt, J.M., Gray, C.M., and Whitehouse, M.J., 2007, Magmatic and crustal differentiation history of granitic rocks from Hf-O isotopes in zircon: Science, v. 315, p. 980–983, doi:10.1126/science.1136154.

Knesel, K.M., and Davidson, J.P., 1996, Isotopic disequilibrium during melting of granite and implications for crustal contamination of magmas: Geology, v. 24, no. 3, p. 243–246, doi:10.1130/0091-7613(1996)024<0243:IDDMOG>2.3.CO;2.

Knesel, K.M., and Davidson, J.P., 2002, Insights into collisional magmatism from isotopic fingerprints of melting reactions: Science, v. 296, no. 5576, p. 2206–2208, doi:10.1126/science.1070622.

Laumonier, M., Scaillet, B., Pichavant, M., Champallier, R., Andujar, J., and Arbaret, L., 2014, On the conditions of magma mixing and its bearing on andesite production in the crust: Nature Communications, v. 5, p. 5607, doi:10.1038/ncomms6607.

Li, Y.J., Wei, J.H., Santosh, M., Tan, J., Fu, L.B., and Zhao, S.Q., 2016, Geochronology and petrogenesis of Middle Permian S-type granitoid in southeastern Guangxi Province, South China: Implications for closure of the eastern Paleo-Tethys: Tectonophysics, v. 682, p. 1–16, doi:10.1016/j.tecto.2016.05.048.

Liang, X.-Q., and Li, X.-H., 2005, Late Permian to Middle Triassic sedimentary records in Shiwandashan Basin: Implication for the Indosinian Yunkai orogenic belt, South China: Sedimentary Geology, v. 177, no. 3-4, p. 297–320, doi:10.1016/j.sedgeo.2005.03.009.

López-Carmona, A., Abati, J., and Reche, J., 2010, Petrologic modeling of chloritoid–glaucophane schists from the NW Iberian Massif: Gondwana Research, v. 17, no. 2-3, p. 377–391, doi:10.1016/j.gr.2009.10.003.

Mahar, E.M., Baker, J.M., Powell, R., Holland, T., and Howell, N., 1997, The effect of Mn on mineral stability in metapelites: Journal of Metamorphic Geology, v. 15, p. 223–238, doi:10.1111/j.1525-1314.1997.00011.x.

Manley, C.R., and Bacon, C.R., 2000, Rhyolite thermobarometry and the shallowing of the magma reservoir, Coso volcanic field, California: Journal of Petrology, v. 41, no. 1, p. 149–174, doi:10.1093/petrology/41.1.149.

Neiva, A.M.R., Silva, P.B., Corfu, F., and Ramos, J.M.F., 2011, Sequential melting and fractional crystallization: Granites from Guarda-Sabugal area, central Portugal: Chemie der Erde: Geochemistry, v. 71, no. 3, p. 227–245.

Neogi, S., Bolton, E.W., and Chakraborty, S., 2014, Timescales of disequilibrium melting in the crust: Constraints from modelling the distribution of multiple trace elements and a case study from the Lesser Himalayan rocks of Sikkim: Contributions to Mineralogy and Petrology, v. 168, no. 2, p. 1020, doi:10.1007/s00410-014-1020-8.

Nicoli, G., Stevens, G., Moyen, J.F., and Frei, D., 2015, Rapid evolution from sediment to anatectic granulite in an Archean continental collision zone: The example of the Bandelierkop Formation metapelites, South marginal zone, Limpopo belt, South Africa: Journal of Metamorphic Geology, v. 33, no. 2, p. 177–202, doi:10.1111/jmg.12116.

Patiño-Douce, A.E., and Beard, J.S., 1996, Effects of P, $f(O_2)$ and Mg/Fe ratio on dehydration melting of model metagreywackes: Journal of Petrology, v. 37, no. 5, p. 999–1024, doi:10.1093/petrology/37.5.999.

Phillips, G. N., Wall, V. J., and Clemens, J., 1981, Petrology of the Strathbogie batholith: A cordierite-bearing granite: Canadian Mineralogist, v. 1981, no. 19, p. 47–63.

Qi, C.S., Deng, X.G., Li, W.X., Li, X.H., Yang, Y.H., and Xie, L.W., 2007, Origin of the Darongshan-Shiwandashan S-type granitoid belt from southeastern Guangxi: Geochemical and Sr-Nd-Hf isotopic constraints: Yanshi Xuebao, v. 23, no. 2, p. 403–412.

Qiao, L., Wang, Q., and Li, C., 2015, The western segment of the suture between the Yangtze and Cathaysia blocks: Constraints from inherited and co-magmatic zircons from Permian S-type granitoids in Guangxi, South China: Terra Nova, v. 27, no. 5, p. 392–398, doi:10.1111/ter.12171.

Rapp, R.P., and Watson, E.B., 1995, Dehydration melting of metabasalt at 8–32 kbar: Implications for continental growth and crust-mantle recycling: Journal of Petrology, v. 36, no. 4, p. 891–931, doi:10.1093/petrology/36.4.891.

Roger, F., Maluski, H., Leyreloup, A., Lepvrier, C., and Truong Thi, P., 2007, U-Pb dating of high temperature metamorphic episodes in the Kon Tum Massif (Vietnam): Journal of Asian Earth Sciences, v. 30, no. 3-4, p. 565–572, doi:10.1016/j.jseaes.2007.01.005.

Sakaguchi, A., 1996, High paleogeothermal gradient with ridge subduction beneath the Cretaceous Shimanto accretionary prism, southwest Japan: Geology, v. 24, no. 9, p. 795–798, doi:10.1130/0091-7613(1996)024<0795:HPGWRS>2.3.CO;2.

Sawyer, E.W., Cesare, B., and Brown, M., 2011, When the continental crust melts: Elements, v. 7, no. 4, p. 229–234, doi:10.2113/gselements.7.4.229.

Scaillet, B., Pichavant, M., and Cioni, R., 2008, Upward migration of Vesuvius magma chamber over the past 20,000 years: Nature, v. 455, no. 7210, p. 216–219, doi:10.1038/nature07232.

Sen, S.K., and Bhattacharya, A., 1984, An orthopyroxene-garnet thermometer and its application to the Madras charnockites: Contributions to Mineralogy and Petrology, v. 88, p. 64–71, doi:10.1007/BF00371412.

Shu, L., Faure, M., Wang, B., Zhou, X., and Song, B., 2008, Late Palaeozoic–early Mesozoic geological features of South China: Response to the Indosinian collision events in Southeast Asia: Comptes Rendus Geoscience, v. 340, no. 2-3, p. 151–165, doi:10.1016/j.crte.2007.10.010.

Stenhouse, I., O'Neill, H., and Lister, G., 2010, Diffusion in natural ilmenite: Vienna, Austria, European Geosciences Union General Assembly 2010, Abstracts, p. 343.

Stevens, G., Villaros, A., and Moyen, J.-F., 2007, Selective peritectic garnet entrainment as the origin of geochemical diversity in S-type granites: Geology, v. 35, no. 1, p. 9–12, doi:10.1130/G22959A.1.

Tajčmanová, L., Connolly, J.A.D., and Cesare, B., 2009, A thermodynamic model for titanium and ferric iron solution in biotite: Journal of Metamorphic Geology, v. 27, no. 2, p. 153–165, doi:10.1111/j.1525-1314.2009.00812.x.

Taylor, J., Nicoli, G., Stevens, G., Frei, D., and Moyen, J.F., 2014, The processes that control leucosome compositions in metasedimentary granulites: Perspectives from the Southern marginal zone migmatites, Limpopo belt, South Africa: Journal of Metamorphic Geology, v. 32, no. 7, p. 713–742, doi:10.1111/jmg.12087.

Vernon, R.H., 2014, Microstructures of microgranitoid enclaves and the origin of S-type granitoids: Australian Journal of Earth Sciences, v. 61, no. 2, p. 227–239, doi:10.1080/08120099.2014.886623.

Vielzeuf, D., and Holloway, J.R., 1988, Experimental determination of the fluid-absent melting relations in the pelitic system: Contributions to Mineralogy and Petrology, v. 98, p. 257–276, doi:10.1007/BF00375178.

Vielzeuf, D., and Montel, J.M., 1994, Partial melting of metagreywackes: Part I. Fluid-absent experiments and phase relationships: Contributions to Mineralogy and Petrology, v. 117, p. 375–393, doi:10.1007/BF00307272.

Villaseca, C., Downes, H., Pin, C., and Barbero, L., 1999, Nature and composition of the Lower continental crust in central Spain and the granulite-granite linkage: Inference from granulitic xenoliths: Journal of Petrology, v. 40, no. 10, p. 1465–1496, doi:10.1093/petroj/40.10.1465.

Wall, V.J., Clemens, J., and Clarke, D.B., 1987, Models of granitoid evolution and source compositions: The Journal of Geology, v. 95, no. 6, p. 731–749, doi:10.1086/629174.

Wan, Y., Liu, D., Wilde, S.A., Cao, J., Chen, B., Dong, C., Song, B., and Du, L., 2010, Evolution of the Yunkai terrane, South China: Evidence from SHRIMP zircon U-Pb dating, geochemistry and Nd isotope: Journal of Asian Earth Sciences, v. 37, no. 2, p. 140–153, doi:10.1016/j.jseaes.2009.08.002.

Watt, G.R., and Harley, S.L., 1993, Accessory phase controls on the geochemistry of crustal melts and restites produced during water-undersaturated partial melting: Contributions to Mineral and Petrology, v. 114, p. 550-566.

White, R.W., and Powell, R., 2002, Melt loss and the preservation of granulite facies mineral assemblages: Journal of Metamorphic Geology, v. 20, p. 621–632.

White, R.W., Powell, R., and Holland, T., 2001, Calculation of partial melting equilibria in the system Na_2O-CaO-K_2O-FeO-MgO-Al_2O_3-SiO_2–H_2O (NCKFMASH): Journal of Petrology, v. 19, p. 139–153.

Whitney, D.L., and Evans, B.W., 2010, Abbreviations for names of rock-forming minerals: American Mineralogist, v. 95, no. 1, p. 185–187.

Zeng, L., Asimow, P.D., and Saleeby, J.B., 2005, Coupling of anatectic reactions and dissolution of accessory phases and the Sr and Nd isotope systematics of anatectic melts from a metasedimentary source: Geochimica et Cosmochimica Acta, v. 69, no. 14, p. 3671–3682, doi:10.1016/j.gca.2005.02.035.

Zhao, G., 2014, Jiangnan orogen in South China: Developing from divergent double subduction: Gondwana Research, v. 27, no. 3, p. 1173–1180, doi:10.1016/j.gr.2014.09.004.

Zhao, K., Xu, X.S., and Erdmann, S., 2017, Crystallization conditions of peraluminous charnockites: Constraints from mineral thermometry and thermodynamic modeling: Contributions to Mineralogy and Petrology, v. 172, p. 26, doi:10.1007/s00410-017-1344-2.

Zhao, L., Guo, F., Fan, W., Li, C., Qin, X., and Li, H., 2010, Crustal evolution of the Shiwandashan area in South China: Zircon U-Pb-Hf isotopic records from granulite enclaves in Indo-Sinian granites: Chinese Science Bulletin, v. 55, no. 19, p. 2028–2038, doi:10.1007/s11434-010-3225-1.

Zhao, L., Guo, F., Fan, W., Li, C., Qin, X., and Li, H., 2012, Origin of the granulite enclaves in Indo-Sinian peraluminous granites, South China, and its implication for crustal anatexis: Lithos, v. 150, p. 209–226, doi:10.1016/j.lithos.2012.02.015.

Zi, J.-W., Cawood, P.A., Fan, W.-M., Wang, Y.-J., Tohver, E., McCuaig, T.C., and Peng, T.-P., 2012, Triassic collision in the Paleo-Tethys Ocean constrained by volcanic activity in SW China: Lithos, v. 144–145, p. 145–160, doi:10.1016/j.lithos.2012.04.020.

Zou, H.B., 1998, Trace element fractionation during modal and nonmodal dynamic melting and open-system melting: A mathematical treatment: Geochimica et Cosmochimica Acta, v. 62, no. 11, p. 1937–1945, doi:10.1016/S0016-7037(98)00115-X.

Zou, H.B., 2000, Modeling of trace element fractionation during non-modal dynamic melting with linear variations in mineral/melt distribution coefficient: Geochimica et Cosmochimica Acta, v. 64, no. 6, p. 1095–1102, doi:10.1016/S0016-7037(99)00383-X.

Science Editor: Aaron J. Cavosie
Associate Editor: Haibo Zou

Manuscript Received 24 November 2016
Revised Manuscript Received 22 March 2017
Manuscript Accepted 4 May 2017

Printed in the USA